united nations educational, scientific and cultural organization

international atomic energy agency

the
abdus salam
international centre for theoretical physics

SMR.1227 - 6

SUMMER SCHOOL ON ASTROPARTICLE PHYSICS AND COSMOLOGY

12 - 30 June 2000

PARTICLE AND ASTROPHYSICS ASPECTS OF ULTRAHIGH ENERGY COSMIC RAYS

Lecture V

G. SIGL
DARC
Observatoire de Paris-Meudon
Meudon
FRANCE

4.) Cosmic Rays as Tools to "Measure" Cosmic Magnetic Fields

a) Magnetic fields influence EM cascades via $e^{\pm}$ synchrotron loss

• In case of γ-rays produced as secondaries by nucleons undergoing pion production, there is a characteristic "cross-over" energy E_c between domination by synchrotron loss and by inverse Compton scattering. E_c only depends on the average extragalactic magnetic field (EGMF) strength.

• A solid angle averaged γ/charged cosmic ray flux ratio of $\simeq 10\%$ at $\sim 10\,\mathrm{EeV}$ would hint to the operation of a TD scenario. At the same time, it would place an independent upper limit of $\simeq 10^{-11}\,\mathrm{G}$ on the EGMF on scales of a few to tens of Mpc.

b) Magnetic fields deflect and delay charged particles

• AGASA observed pairs which might stem from bursting sources which cannot be much further away than $\sim 100\,\mathrm{Mpc}$ (due to small attenuation length for the higher energy particle). Future observations with Auger could provide much more statistics. Comparison with Monte Carlo simulations might allow to construct the likelihood function for EGMF parameters and maybe even for distance and activity time scale of the sources.
Bursting TD sources might constitute especially attractive probes.

Energy loss rates of electrons in the EM cascade

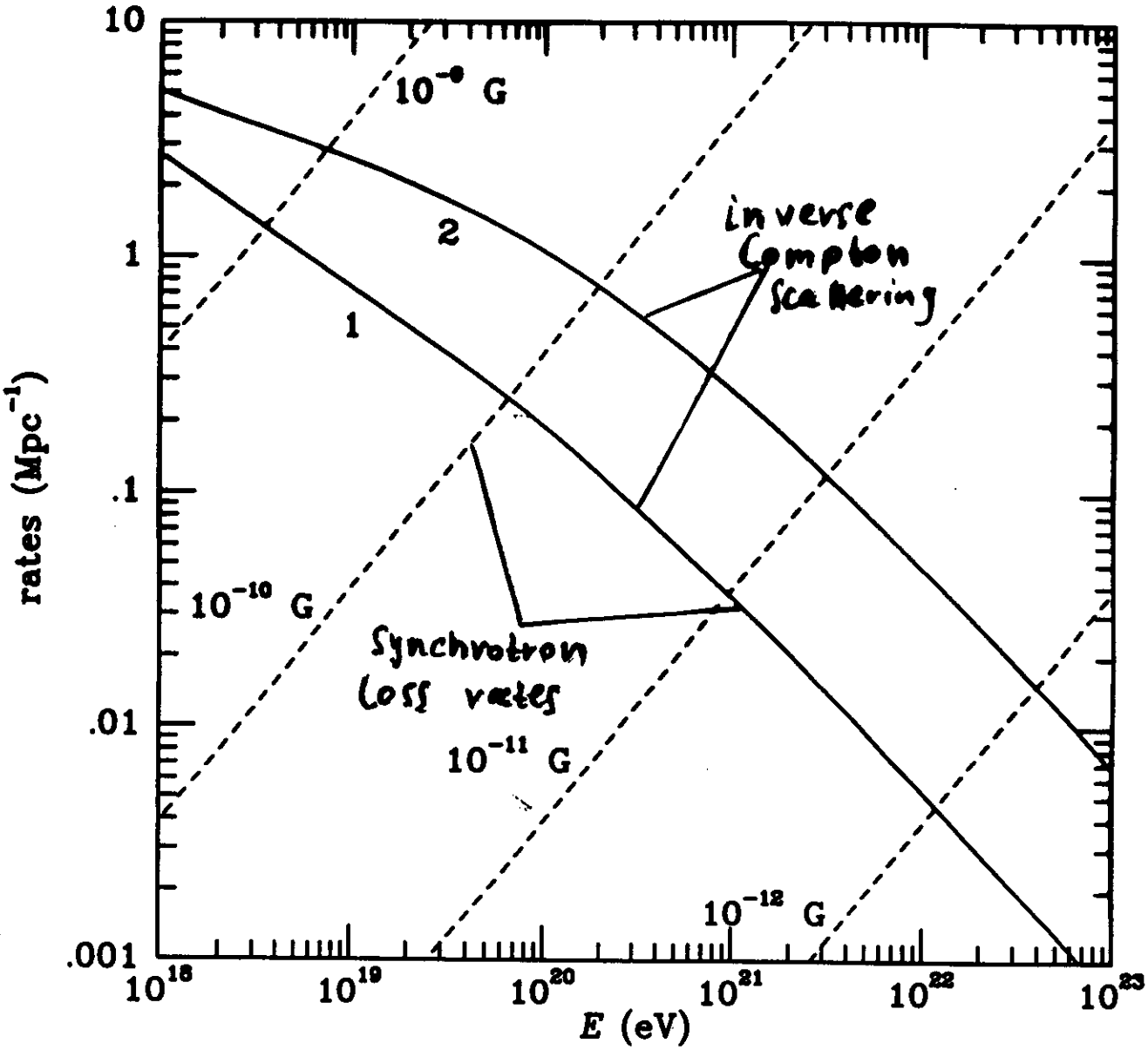

uniform distribution of acceleration sources

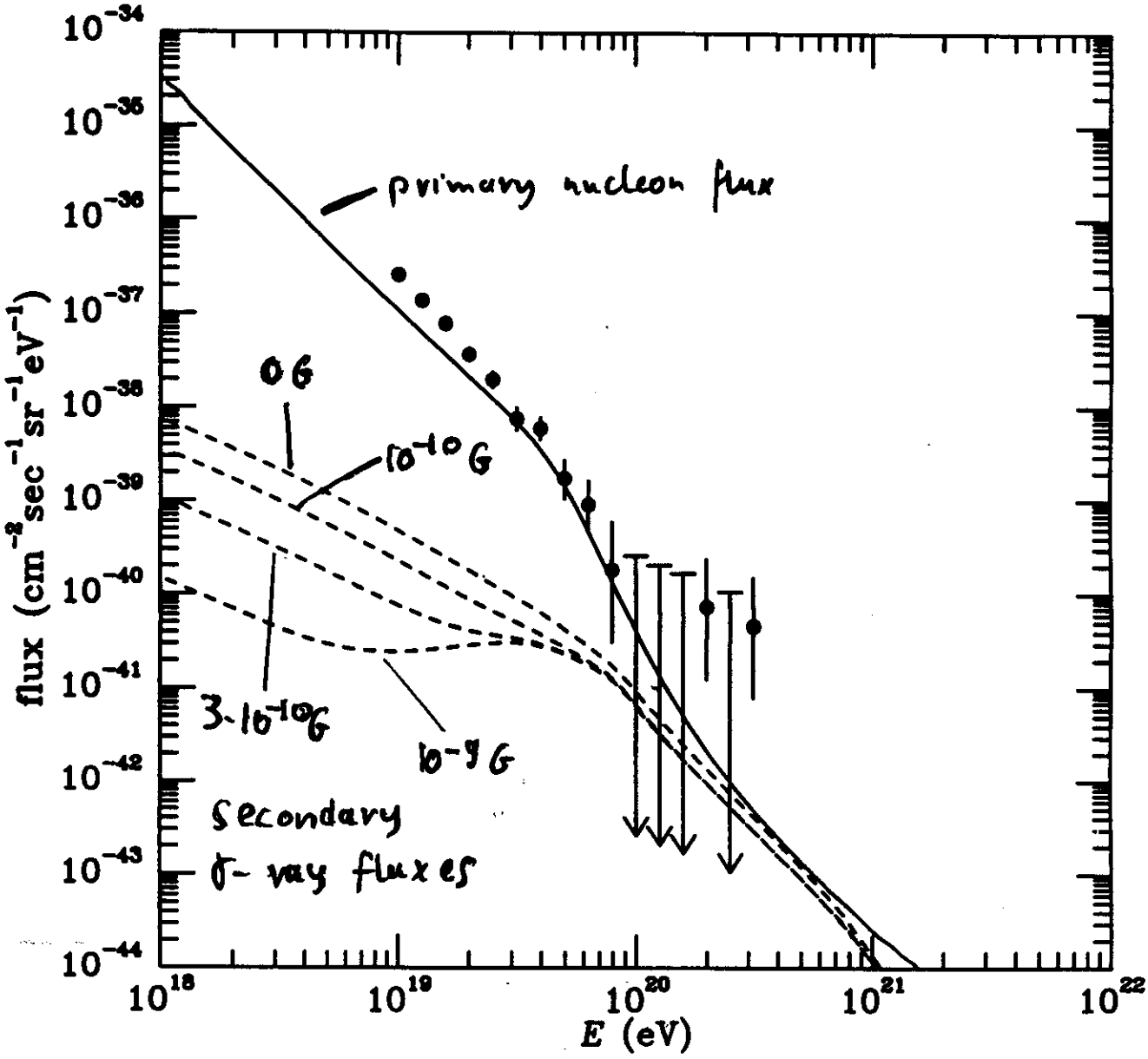

S. Lee, A. V. Olinto, G. S., Ap J. 455 (1995) L21

Implications of AGASA pairs for B (assuming discrete sources)

relative angular deflection for two energies $\lesssim 2.5^\circ$ (resolution)

$$\Rightarrow B_{rms} \lesssim 5 \cdot 10^{-10} \left(\frac{d}{30\,\mathrm{Mpc}}\right)^{-1/2} \left(\frac{l_c}{1\,\mathrm{Mpc}}\right)^{-1/2} G$$

compare with best limit on large-scale magnetic fields from Faraday rotation of radio wave polarization from high-z sources:

$$B_{rms} \lesssim 10^{-9} \left(\frac{l_c}{1\,\mathrm{Mpc}}\right)^{-1/2} G$$

$\Longrightarrow$ potentially constrains origin of Galactic field: $B_{rms} \sim 10^{-12} - 10^{-9}$ G
if no dynamo, much smaller otherwise

$\longrightarrow$ probes primordial magnetic fields

Angle-Time-Energy Images of Ultrahigh Energy Cosmic Ray Sources

assume:

- particle of charge Z, energy E
- (homogeneous) statistical description of magnetic field: strength B_{rms}, coherence scale L_c

=) average time delay

$$\bar{\tau}_E \simeq \frac{\alpha_{rms}^2 d}{4} \simeq 2 \left(\frac{d}{30\,\mathrm{Mpc}}\right)^2 \left(\frac{E}{10^{20}\,\mathrm{eV}}\right)^{-2} \left(\frac{B_{rms}}{10^{-11}\,\mathrm{G}}\right)^2 \left(\frac{l_c}{1\,\mathrm{Mp}}\right) \mathrm{yr}$$

in general 3 time scales involved:

delay time $\bar{\tau}_E$, emission time scale T_s, experimental Lifetime T_{obs}

Distributions sensitive to RELATIVE SIZE

Next step: include localized regions of strong magnetic fields

M. Lemoine, G.S., P Biermann

Assume

- particle of charge Z and energy E
- magnetic field of strength B_{rms} and coherence length l_c

Then average time delay over distance $d \gtrsim l_c$ is

$$\tau_E \simeq \frac{\alpha_{rms}^2 d}{4} \simeq 2 \left(\frac{d}{30\,\mathrm{Mpc}}\right)^2 \left(\frac{E}{100\,\mathrm{EeV}}\right)^{-2} \left(\frac{B_{rms}}{10^{-9}\,\mathrm{G}}\right)^2 \left(\frac{l_c}{1\,\mathrm{Mpc}}\right) \mathrm{yr}$$

Assume observed clusters of events stem from a discrete source

Define likelihood function

$$\mathcal{L}(\tau_{100}, T_S, d, \gamma, N_0, l_c, n_B) = \left\langle \prod_{j=1}^{N} e^{-s_j} \frac{s_j^{n_j}}{n_j!} \right\rangle$$

j : energy-time bin (no angular binning here)

s_j : predicted $\nu\nu$ events in bin j

n_j : observed " " " "

T_S: source emission time scale

γ : injection (power law) spectral index

N_0: total source fluence at detector over infinite time

n_B : magnetic field spectral index

Emission time scale << delay time

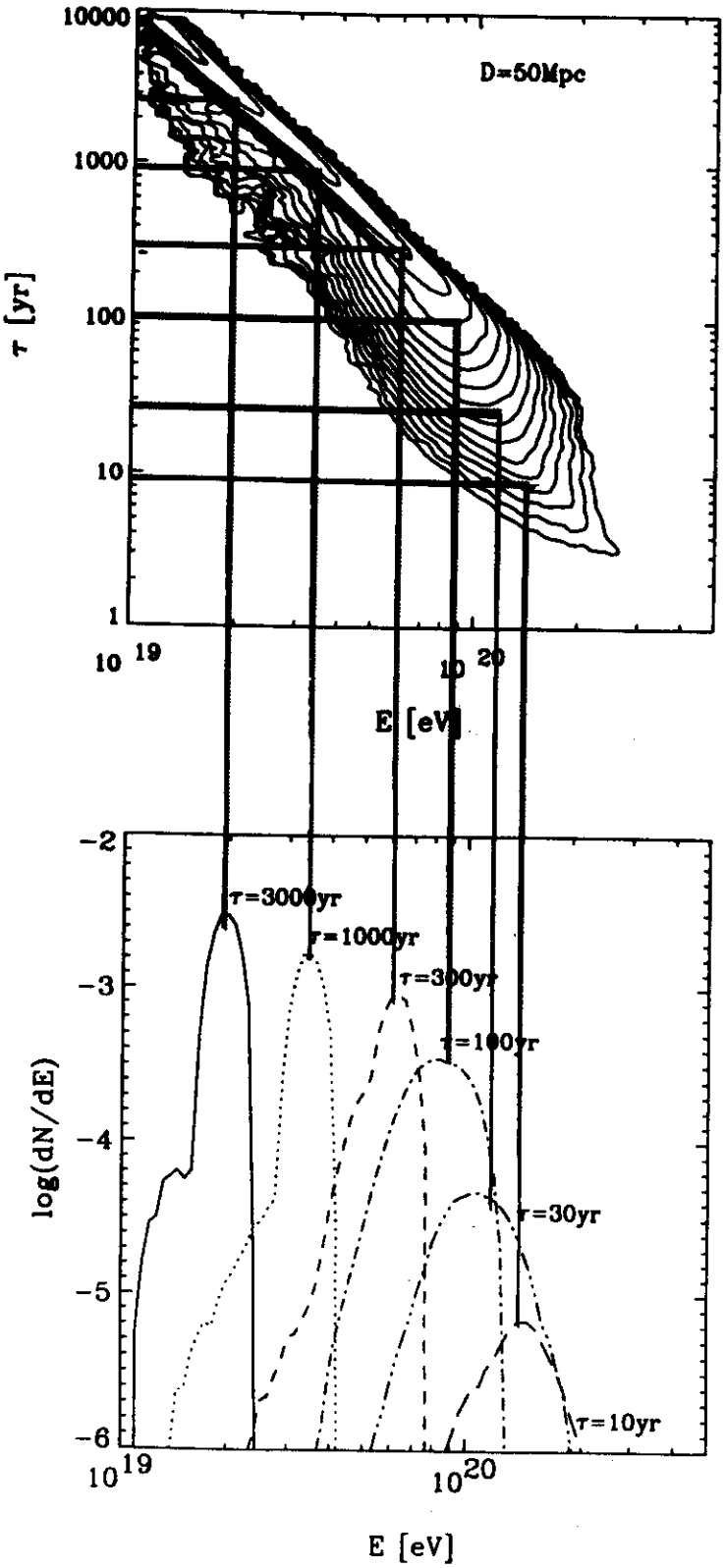

Emission time scale << delay time

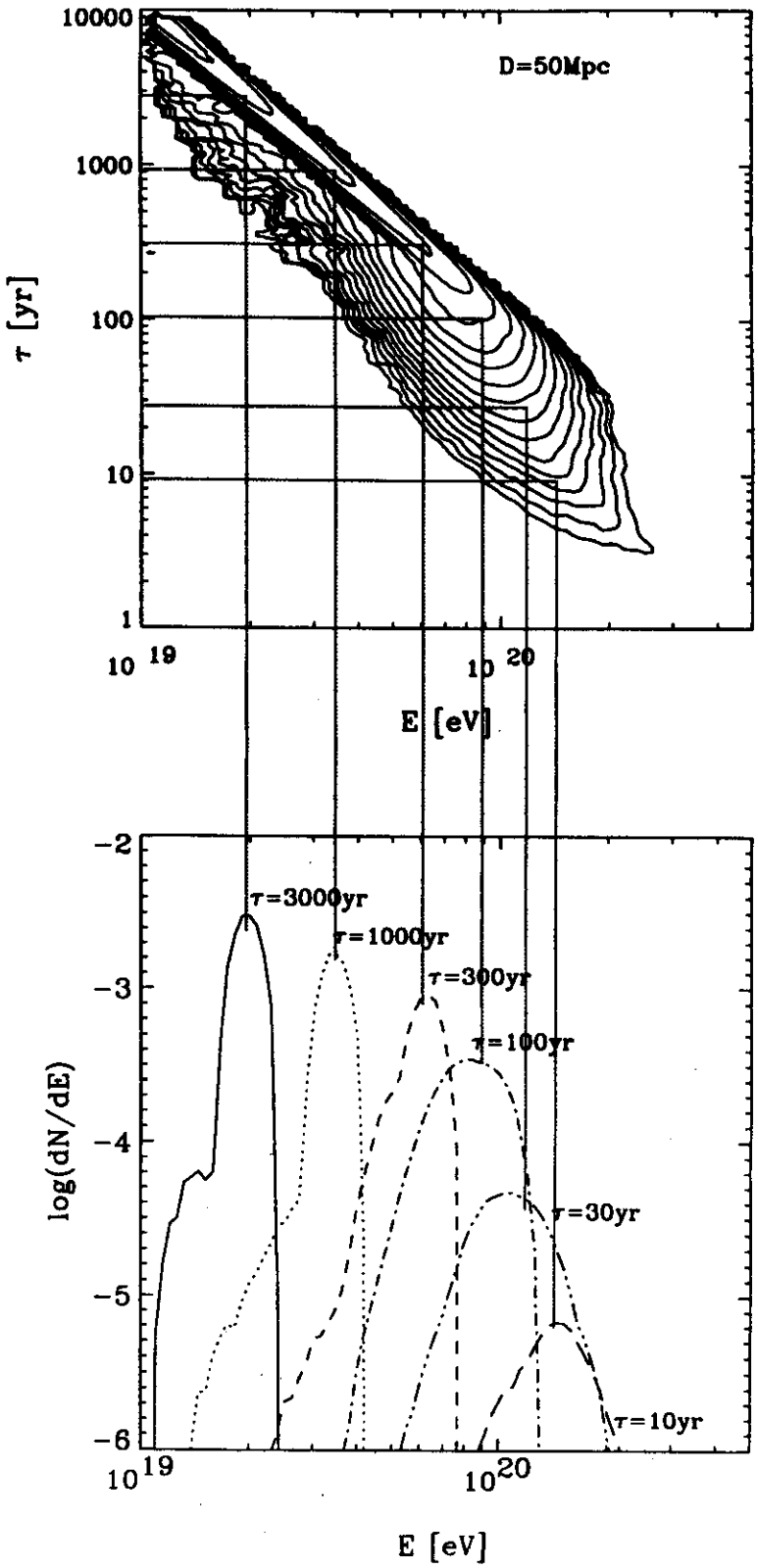

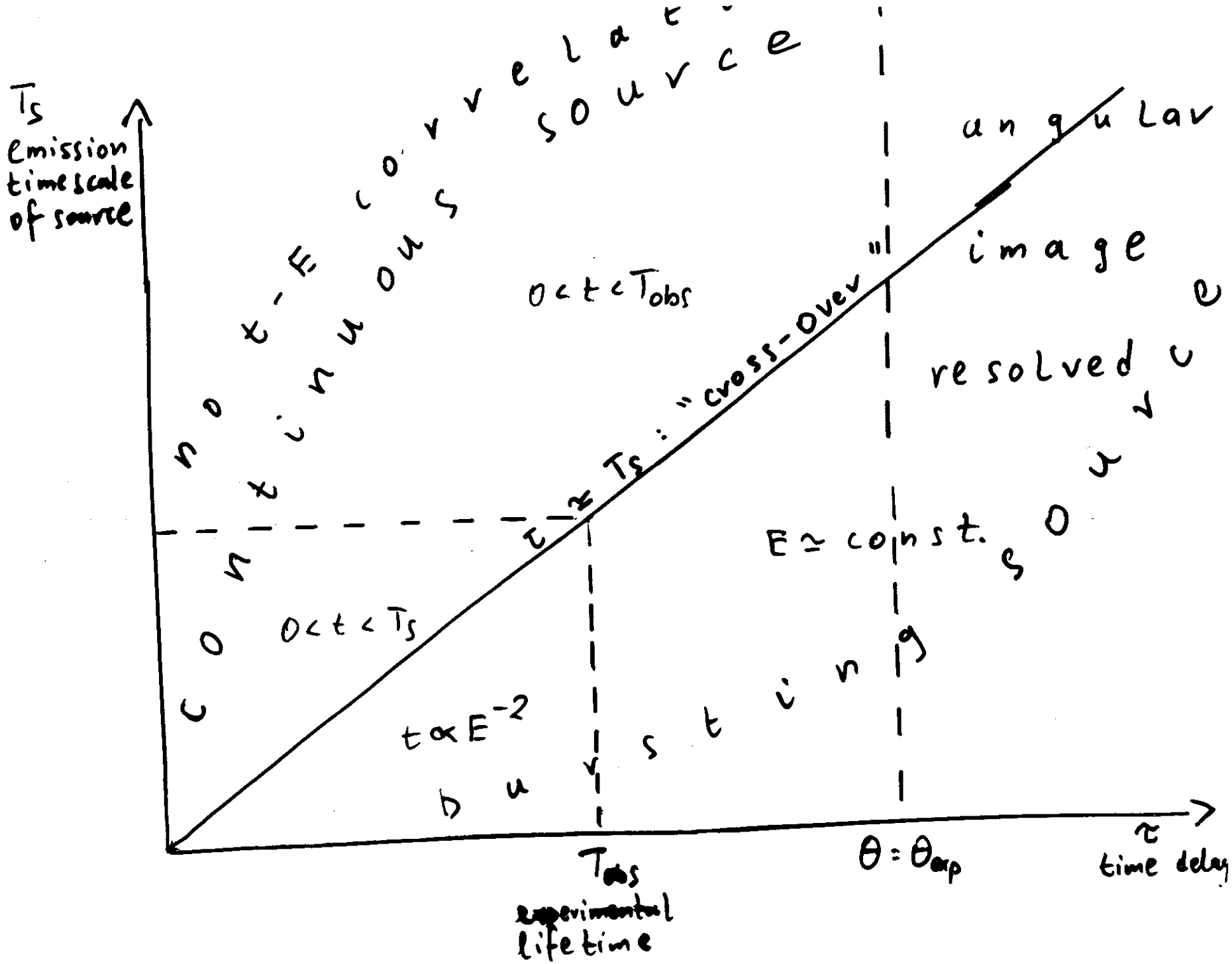
Ts
emission timescale of source
non-correlated source
continuous
0 < t < Tobs
angular image
resolved source
τ ≃ Ts : "cross-over"
E ≃ const.
0 < t < Ts
t ∝ E^-2
bursting
Tobs
experimental lifetime
θ = θexp
τ
time delay

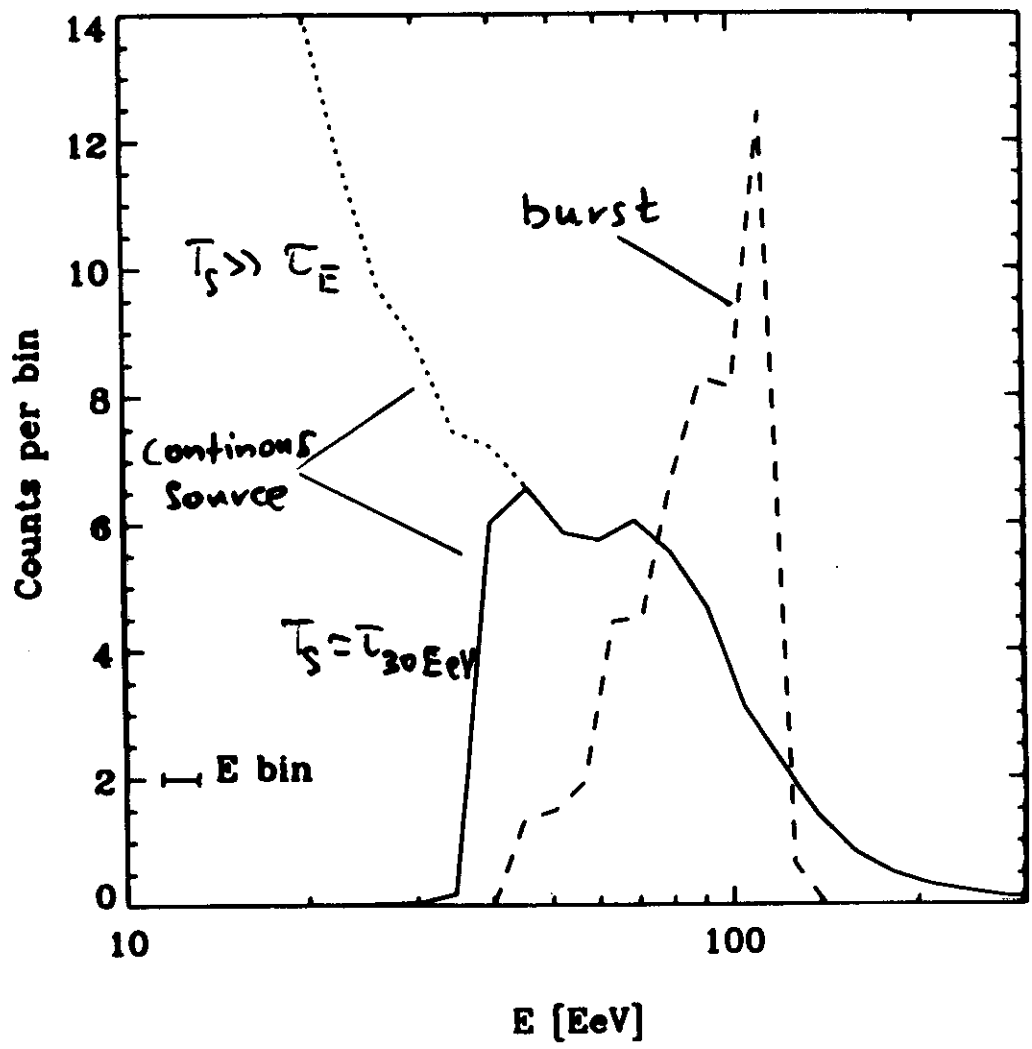

Fig. 3.— Energy spectra for a continuous source (solid line), and for a burst (dashed line). Both spectra are normalized to a total of 50 particles detected. The parameters corresponding to the continuous source case are: $T_S = 10^4\,\mathrm{yr}$, $\tau_{100} = 1.3 \times 10^3\,\mathrm{yr}$, and the time of observation is $t = 9 \times 10^3\,\mathrm{yr}$, relative to propagation with the speed of light. A low energy cutoff results at the energy $E_S = 40\,\mathrm{EeV}$ where $\tau_{E_S} = t$ (see text). The dotted line shows how the spectrum would continue if $T_S \gtrsim 10^4\,\mathrm{yr}$. The case of a bursting source corresponds to a slice of the image in the $\tau_E - E$ plane, as indicated in Figure 1 by dashed lines. For both spectra, $D = 30\,\mathrm{Mpc}$, and $\gamma = 2$.

$\tau_E \gg T_{obs}, \tau_E \gg T_S$; e.g. GRB, topological defect

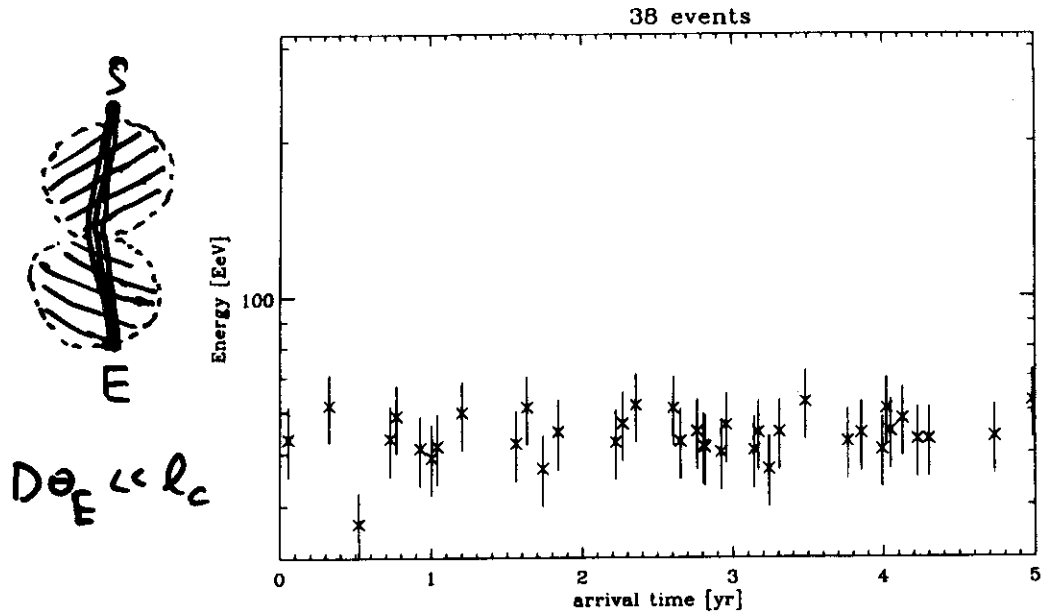

Figure 2: Same as for Fig. 1, except for the parameters $\tau_{100} = 50\,\mathrm{yr}$, and $N_0 = 4 \times 10^3$. This serves as an example for a burst with a long time delay, but still in the limit of small deflection, $D\theta_E/l_c \ll 1$, leading to a small detected energy dispersion.

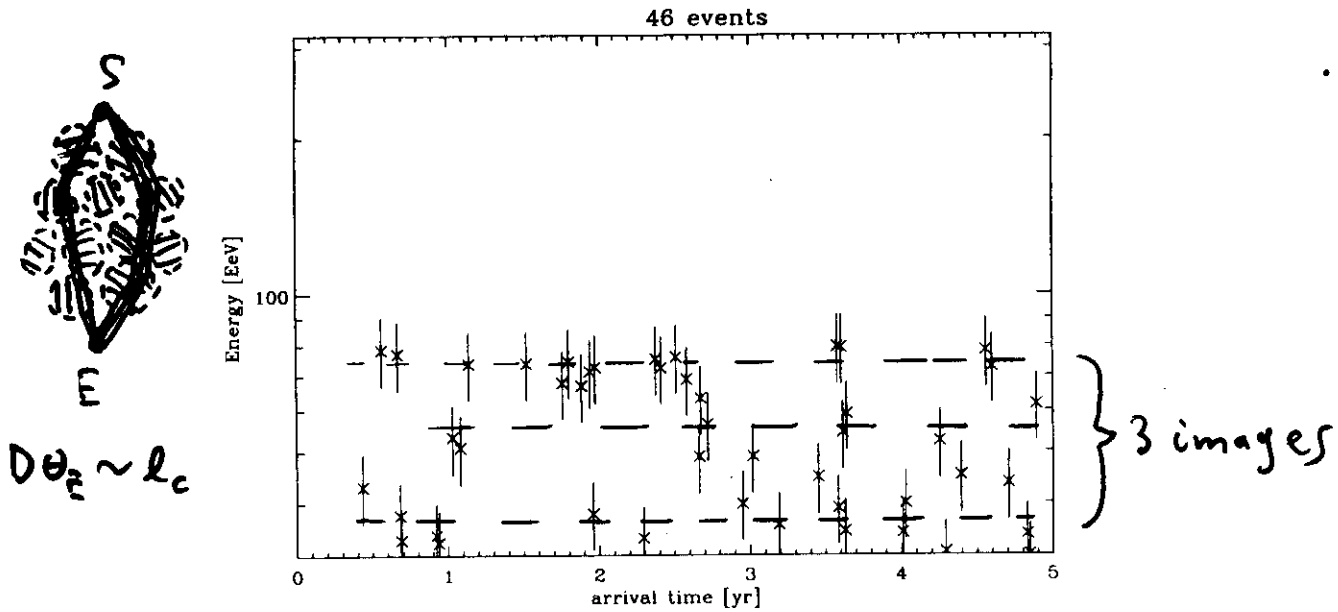

Figure 3: Same as Fig. 1, except for the parameters $\tau_{100} = 250\,\mathrm{yr}$, $N_0 = 2 \times 10^4$, and $l_c \simeq 0.25\,\mathrm{Mpc}$. This serves as an example for a burst with a long time delay for intermediate deflection, $D\theta_E/l_c \sim 1$. The distinct sub-bands are due to multiple source images.

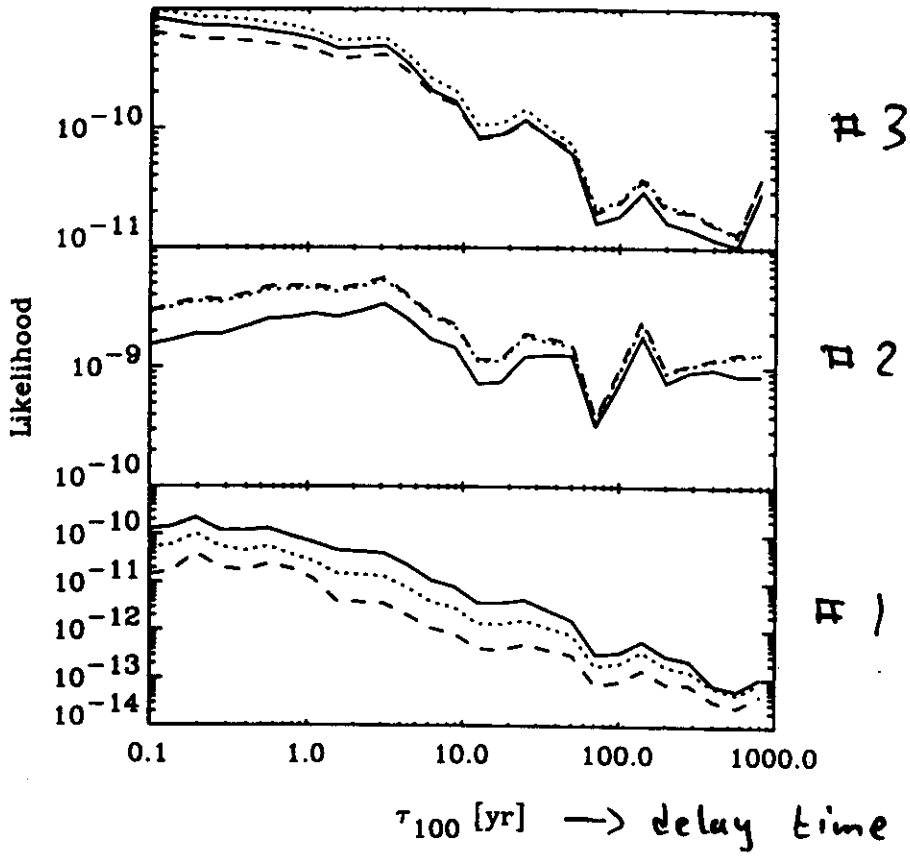

Likelihood marginalized with respect to emission time scale and source fluence.

D = 30 Mpc

——— $\gamma = 1.5$

- - - - - - $\gamma = 2.0$

– – – – $\gamma = 2.5$

Likelihood Function for a cluster with $D\theta_E \sim l$

→ Small coherence length

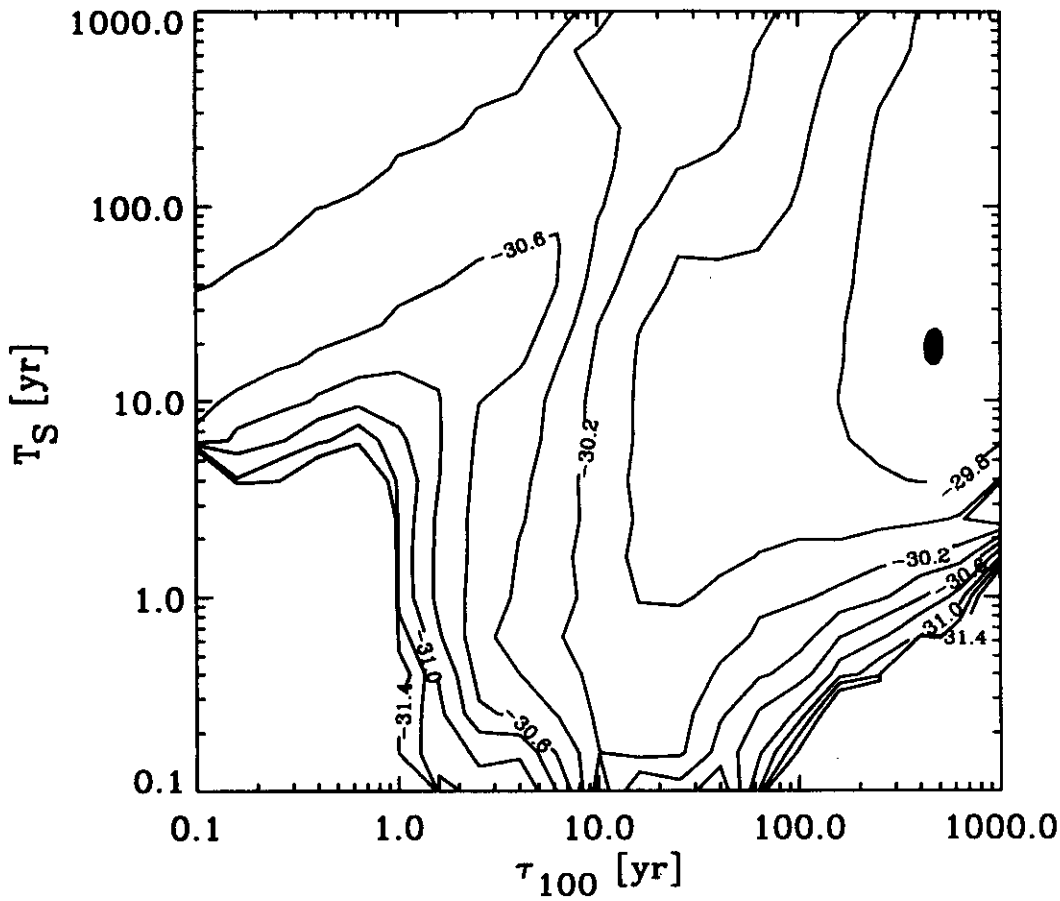

Fig. 7. The likelihood for the cluster shown in Fig. 3, marginalized over N_0 and γ, plotted in the $\tau_{100} - T_S$ plane, for $D = 50\,\mathrm{Mpc}$ and $l_c \simeq 0.25\,\mathrm{Mpc}$ (the true values). The maximum of the likelihood occurs for $\tau_{100} \simeq$ a few hundred years, $T_S \simeq$ a few years which is a good reconstruction of the true values. The contours shown go from the maximum down to values of about 0.01 of the maximum in steps of a factor $10^{0.2} = 1.58$. Note that values in the range $\tau_E = T_S$ with $E \gtrsim 80\,\mathrm{EeV}$ and $T_S \gtrsim 10\,\mathrm{yr}$ are not significantly excluded, as expected (see text). The fall-off at $\tau_{100} \gtrsim 50\,\mathrm{yr}$ and $T_S \lesssim 3\,\mathrm{yr}$ is a numerical artifact due to the limited number of propagated particles (4×10^4 per parameter set) which causes too patchy histograms in arrival time.

Likelihood Function for a cluster with $D\theta_E \sim l_c$

→ large coherence length

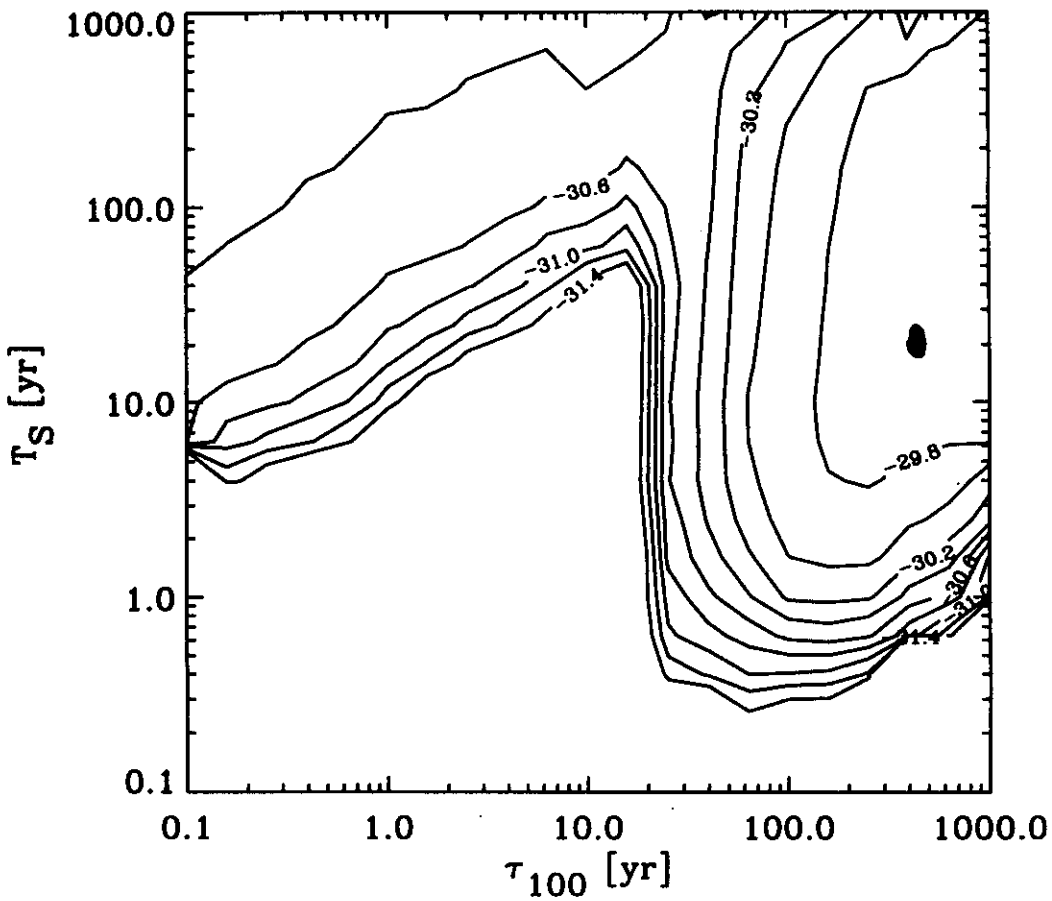

Fig. 11. Same as Fig. 7, but assuming a magnetic field coherence length $l_c \simeq 1$ Mpc. The maximum of the likelihood is near $\tau_{100} = 400$ yr, $T_S = 20$ yr which again is a reasonable reconstruction of the true values. Note that if τ_{100} were known to be smaller than $\simeq 50$ yr, a coherence length as large as l_c [illegible] Mpc could be ruled out, but $l_c \simeq 0.25$ Mpc would be allowed (see Fig. 7 and discussion in the text).

have to increase τ_{100} to satisfy $D\theta_E \sim l_c$

⇒ likelihood function has no power at small τ_{100}

$\tau_E \lesssim T_S$ for all events, e.g. AGN

"cross-over"

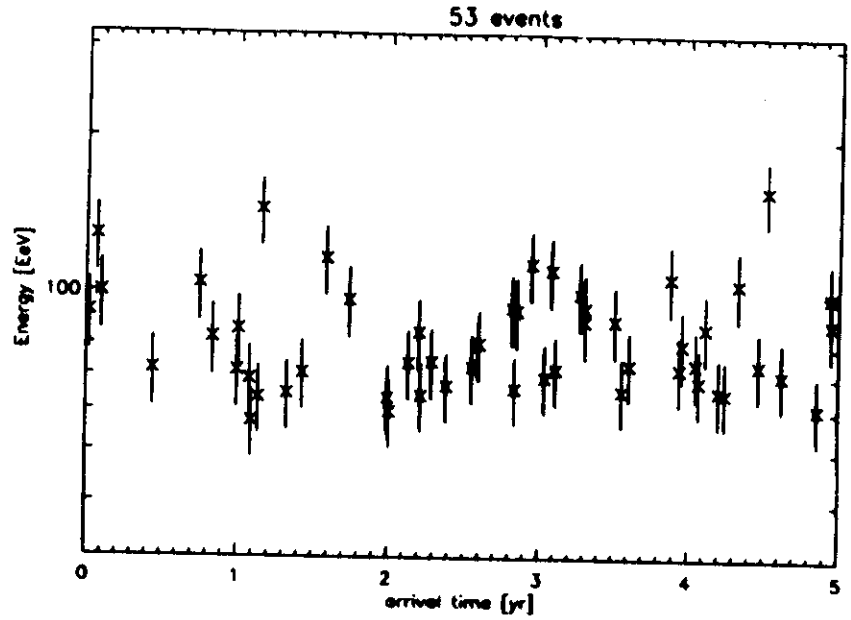

Figure 4: Same as Fig. 1, except for the parameters $\tau_{100} = 50\,\mathrm{yr}$, $T_S = 200\,\mathrm{yr}$, and $N_0 = 1.4 \times 10^4$. A lower cut-off in energy occurs at $E_C \simeq 60\,\mathrm{EeV}$ where $\tau_{E_C} \simeq T_S$.

continuous

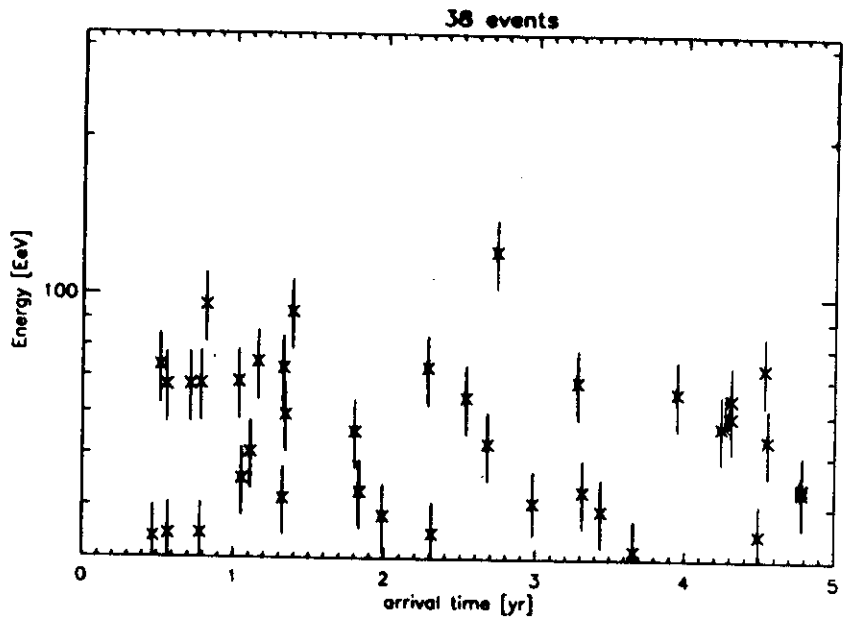

Figure 5: Same as Fig. 1, except for the parameters $\tau_{100} = 0.1\,\mathrm{yr}$, $T_S = 500\,\mathrm{yr}$, and $N_0 = 10^4$. This serves as an example of a source that is continuously emitting at all relevant energies.

(a)

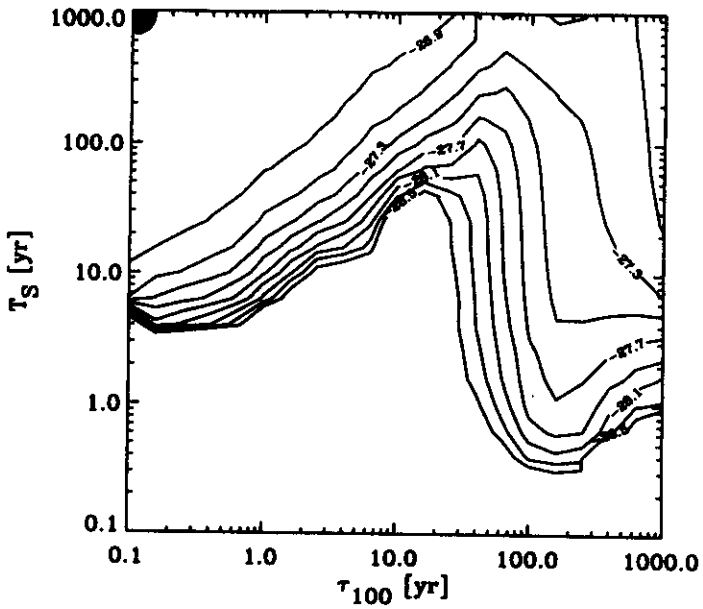

(b)

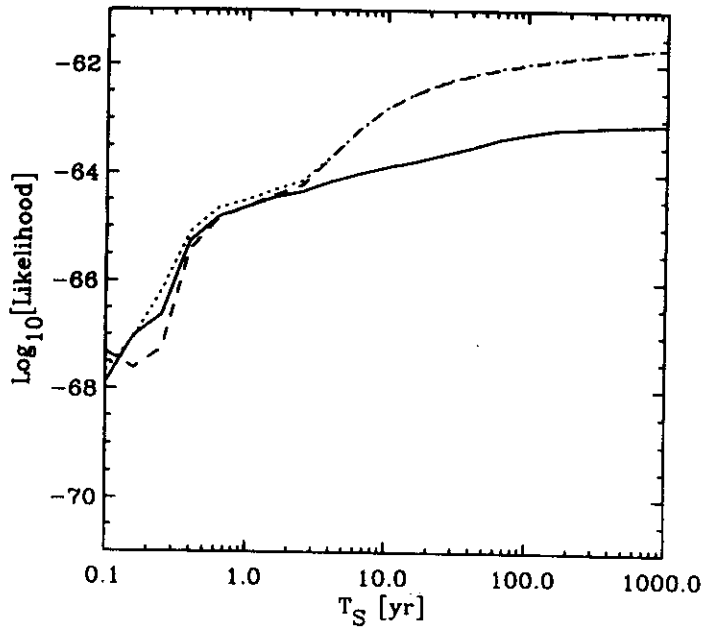

Figure 1: (a) The likelihood for the cluster shown in Fig. 5, marginalized over N_0 and γ, plotted in the $\tau_{100} - T_S$ plane, for $D = 50\,\mathrm{Mpc}$, $l_c \simeq 1\,\mathrm{Mpc}$ (the true values). The maximum of the likelihood is near $\tau_{100} = 0.1\,\mathrm{yr}$, $T_S = 10^3\,\mathrm{yr}$ which is a good reconstruction of the true values. (b) Same as (a), but marginalized over N_0 and τ_{100}, plotted versus the emission timescale T_S. Solid line is for $\gamma = 1.5$, dotted line for $\gamma = 2.0$ (the true value), and dashed line for $\gamma = 2.5$. Parameters in the range $T_S \lesssim 10\,\mathrm{yr}$ and $\tau_{100} \gtrsim 10\,\mathrm{yr}$, that would be typical for a burst with a large time delay, are therefore excluded at about 95% confidence level.

"Cross-over", $\tau_E \simeq T_S \gg T_{obs}$

e.g. hot spots in radio galaxies

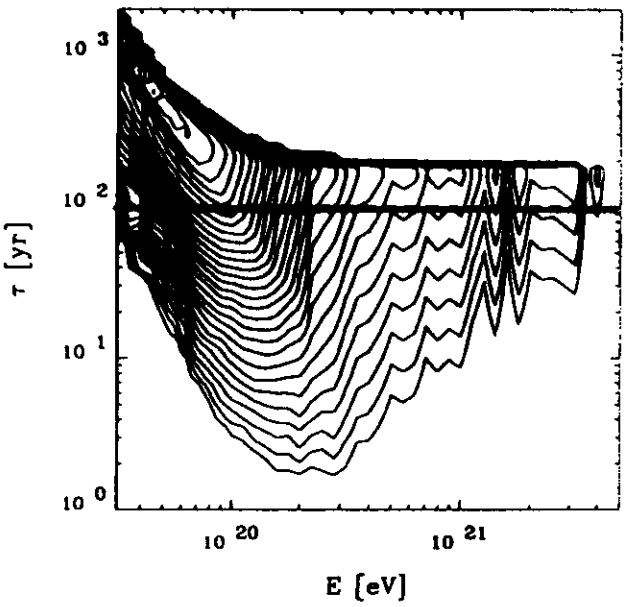

(a)

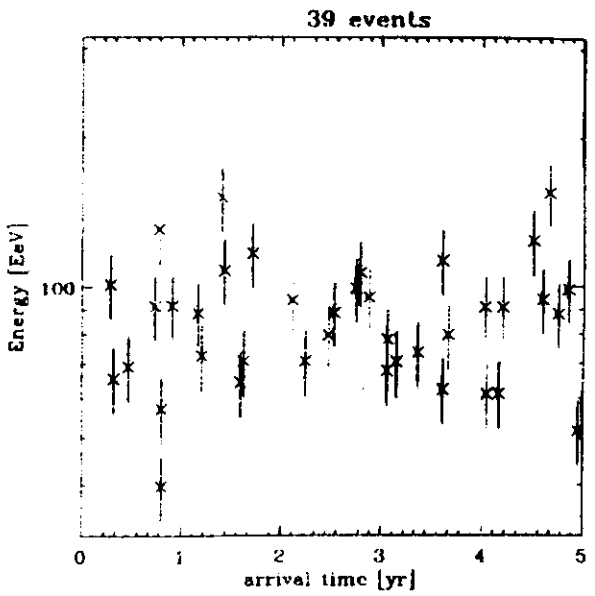

(b)

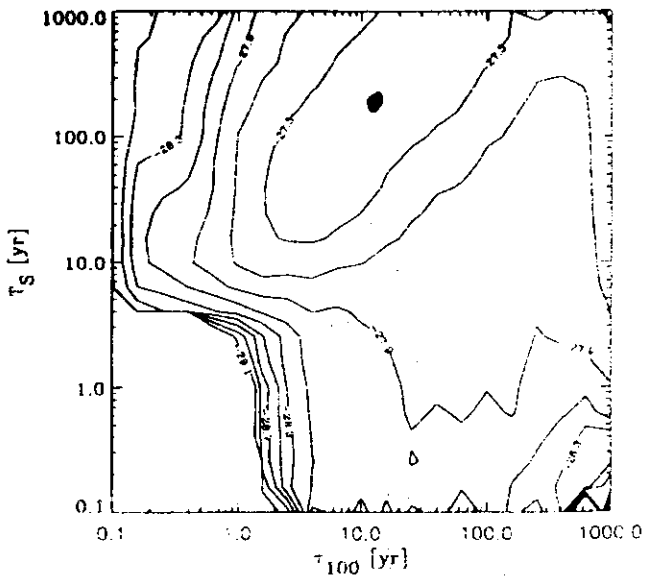

(c)

Low-energy cut-off is a signature for a "cross-over" where

$$\tau_{E_c} \simeq T_S$$

If τ_E is large enough such that deflection angle

$$\theta_E \simeq 2^\circ \left(\frac{d}{10\,\mathrm{Mpc}}\right)^{-1/2} \left(\frac{\tau_E}{10^4\,\mathrm{yr}}\right)^{1/2}$$

can be resolved, $T_S \gg T_{obs}$ can be measured

$$1\cdot 10^3 \left(\frac{\Delta\theta}{1^\circ}\right)^2 \left(\frac{d}{10\,\mathrm{Mpc}}\right) \mathrm{yr} \lesssim T_S \simeq \tau_E \lesssim 10^4 \ldots 10^7 \left(\frac{E}{100\,\mathrm{EeV}}\right)^{-2} \mathrm{yr}$$

↑ angular image resolvable

↑ constraints on magnetic fields, e.g. Faraday rotation

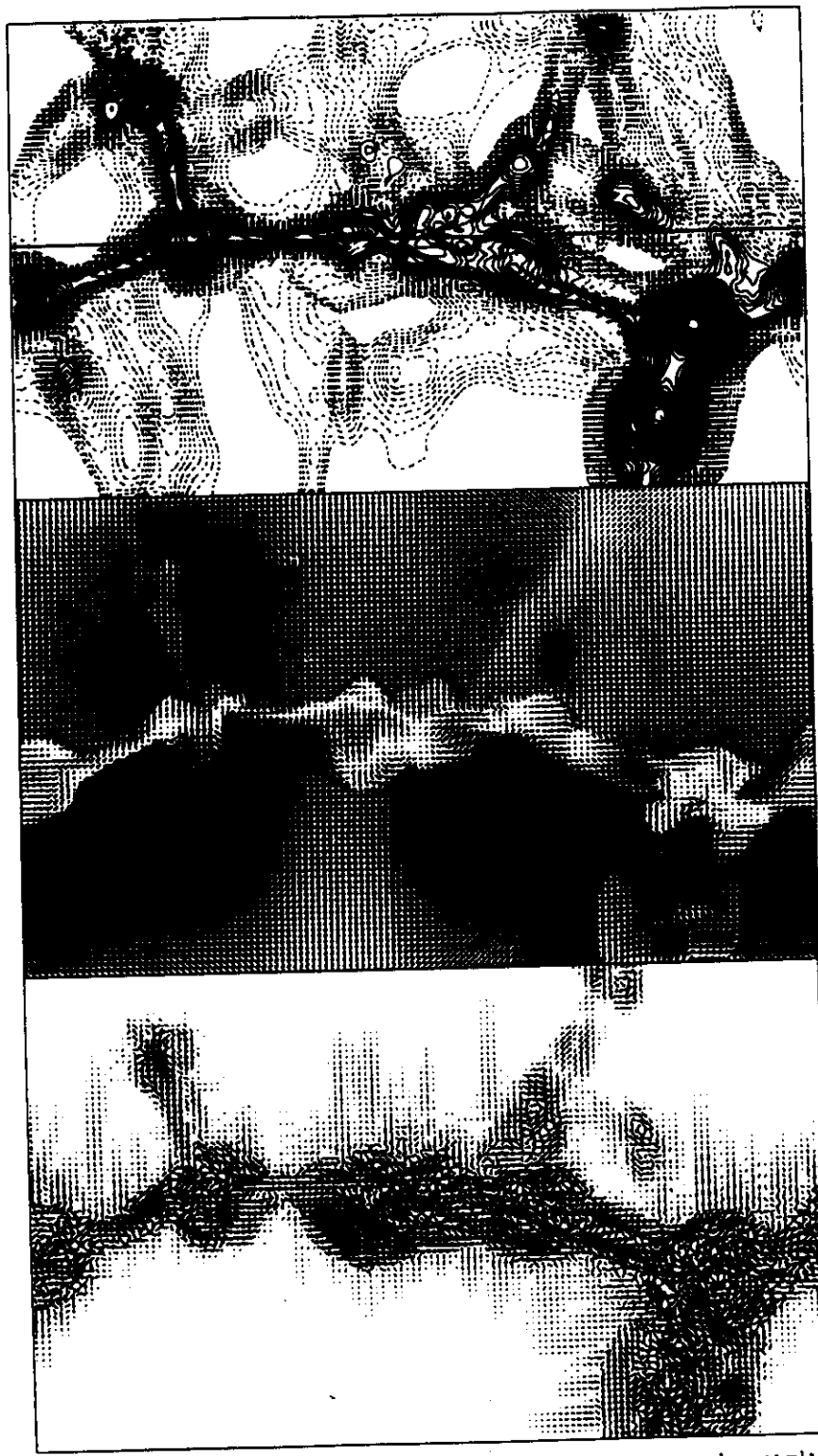

Fig. 1. Two-dimensional cut of the simulated universe at $z = 0$. The plot shows a region of $32h^{-1} \times 20h^{-1}\mathrm{Mpc}^2$ with a thickness of $0.25h^{-1}\mathrm{Mpc}$, although the simulation was done in a box of $(32h^{-1}\mathrm{Mpc})^3$ volume. The first panel shows baryonic density contours, the second panel shows velocity vectors, and the third panel shows magnetic field vectors. In the first panel, the solid lines contour the regions of $\rho_b \geq \bar{\rho}_b$ and the dotted lines contour those of $10^{-1.2}\bar{\rho}_b \leq \rho_b < \bar{\rho}_b$. In the third panel, the vector length is proportional to the log of magnetic field strength.

D = 10 Mpc

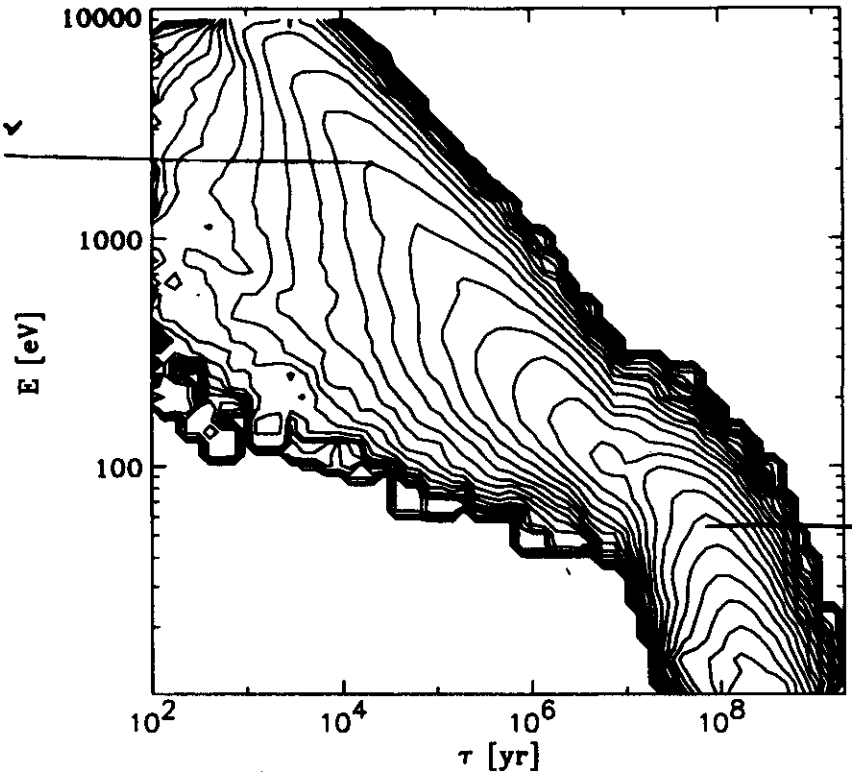

$B_{rms} = 10^{-7}$ G

rectilinear
$\tau_E \propto E^{-2}$

diffusion
$\tau_E \propto E^{-1}$

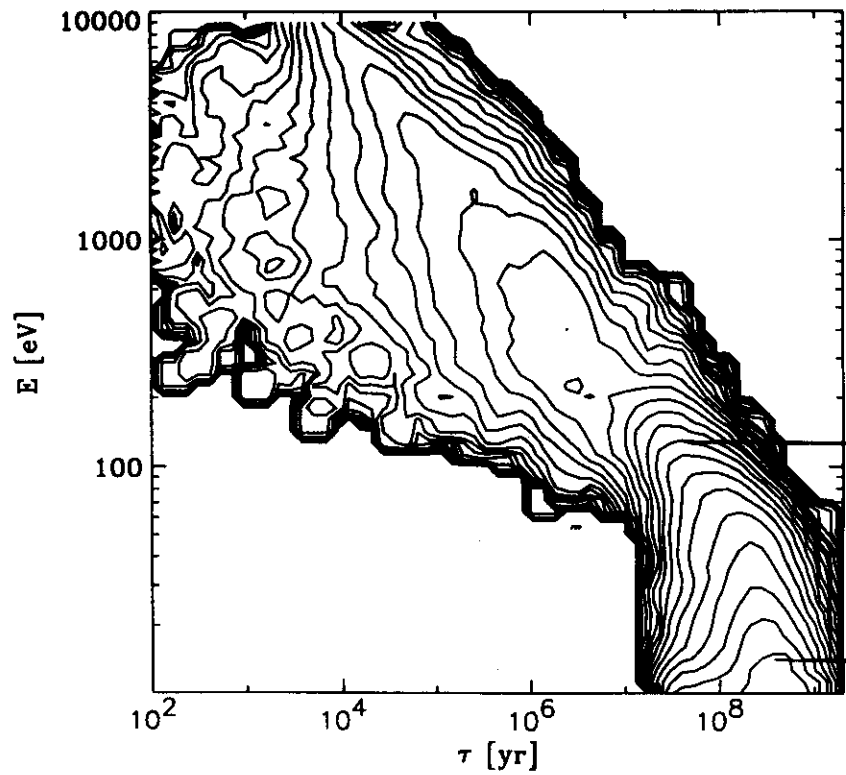

$B_{rms} = 3 \cdot 10^{-7}$ G

$\tau_E \propto E^{-1}$

$\tau_E \propto E^{-1/3}$

Supergalactic plane as a sheet with Gaussian profile, width=10 Mpc

Kolmogorov field with $B_{\rm rms,max} = 10^{-7}\,{\rm G}$, $L_{\rm max} \simeq 10\,{\rm Mpc}$, $l_c \simeq 1\,{\rm Mpc}$

continuous source with $T_{\rm S} \gg \tau_{10} \sim 2 \times 10^8\,{\rm yr}$, $j(E) \propto E^{-2.4}$ up to $10^{22}\,{\rm eV}$, $D = 10\,{\rm Mpc}$

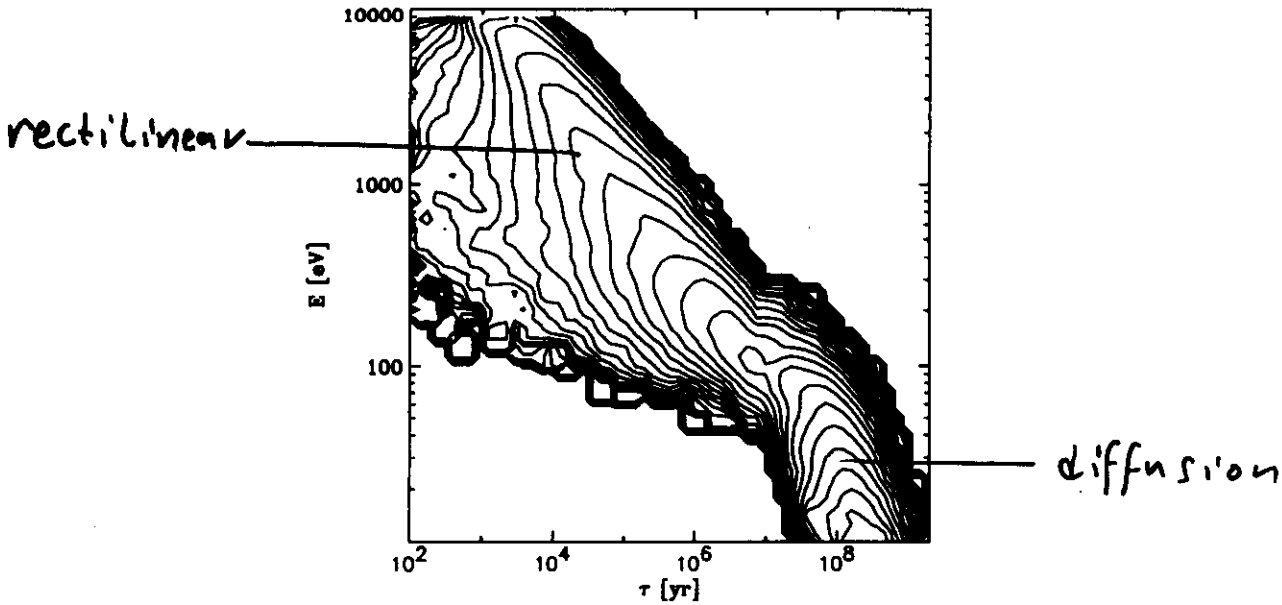

delay time-energy distribution

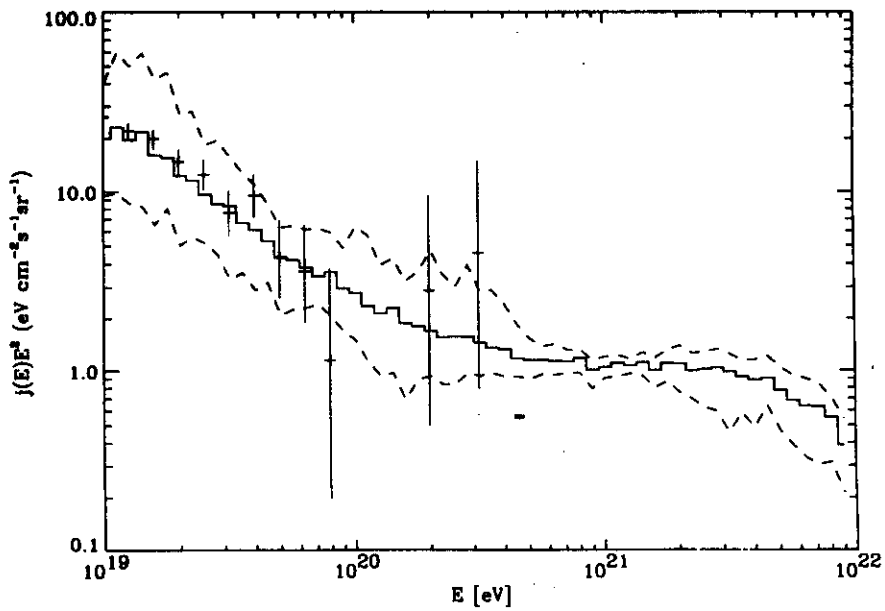

average spectrum and variance: Higher and lower fields produce much poorer fits

Simple Model:

Supergalactic plane as a sheet with thickness $\simeq$ 10 Mpc, typically Gaussian profile
B-field has a Kolmogorov spectrum with $B_{rms,max}$ varied, $L_{max} \simeq 10$ Mpc, $L_c \simeq 1$ Mpc, weighted by density profile

3-field realizations represented on a spatial grid via Fourier transformation

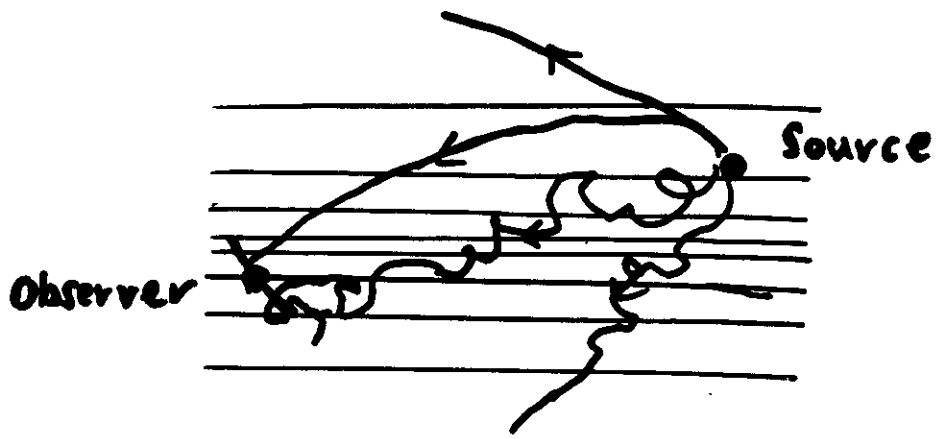

propagate many particles for different realizations
record energies E, delay times τ_E, angles θ, φ

typically continuous source, injection spectrum $\Phi(E) \propto E^{-2.4}$ up to $\simeq 10^{21} - 10^{22}$ eV,

Important Influences / Effects:

- almost rectilinear propagation

  $\tau_E \ll D$

  $$E \gtrsim 10^{20} \left(\frac{D}{10\,\mathrm{Mpc}}\right)^{1/2} \left(\frac{B_{\mathrm{rms}}}{10^{-9}\,\mathrm{G}}\right) \left(\frac{\ell_c}{1\,\mathrm{Mpc}}\right) \mathrm{eV}$$

  then $j(E) \propto \frac{\Phi(E)}{4\pi D^2} \lambda(E)$

- opposite limit: diffusive regime

  $$j(E) \propto \Phi(E)\, \tau_E \propto \Phi(E) / D(E)$$

  in equilibrium and up to energy losses

- energy losses, especially pion production (GZK effect)

  tends to increase low energy flux, especially if diffusive regime reaches beyond $E_{GZK} \simeq 7 \cdot 10^{19}$ eV

- inhomogeneity suppresses low energy flux within strong field regions (escape?)

  mostly dependent on D, inhomogeneity length scale and contrast, less on profiles

Approximation in diffusive regime

solve diffusion - continuous energy loss equation

$$\partial_t n(\vec{r}, E, t) = + \vec{\nabla} \cdot [D(\vec{r}, E)\, \vec{\nabla} n(\vec{r}, E, t)] - \partial_E [b(E)\, n(\vec{r}, E, t)] + \Phi(\vec{r}, E, t)$$

partial differential equation

integrate over age of Universe $\simeq O(10^{10}\,\text{yr})$

$\longrightarrow$ usually reach equilibrium if $\Phi(t)$ and $\tau_E \lesssim 10^{10}\,\text{yr}$

- analytical (Syrovatsky) solution if homogeneous $\rightarrow$ P.B.
- otherwise numerical

Warning: pion production is stochastic, not continuous, especially for $D \lesssim 10\,\text{Mpc}$

$B_{rms} = 5 \cdot 10^{-8}$ G

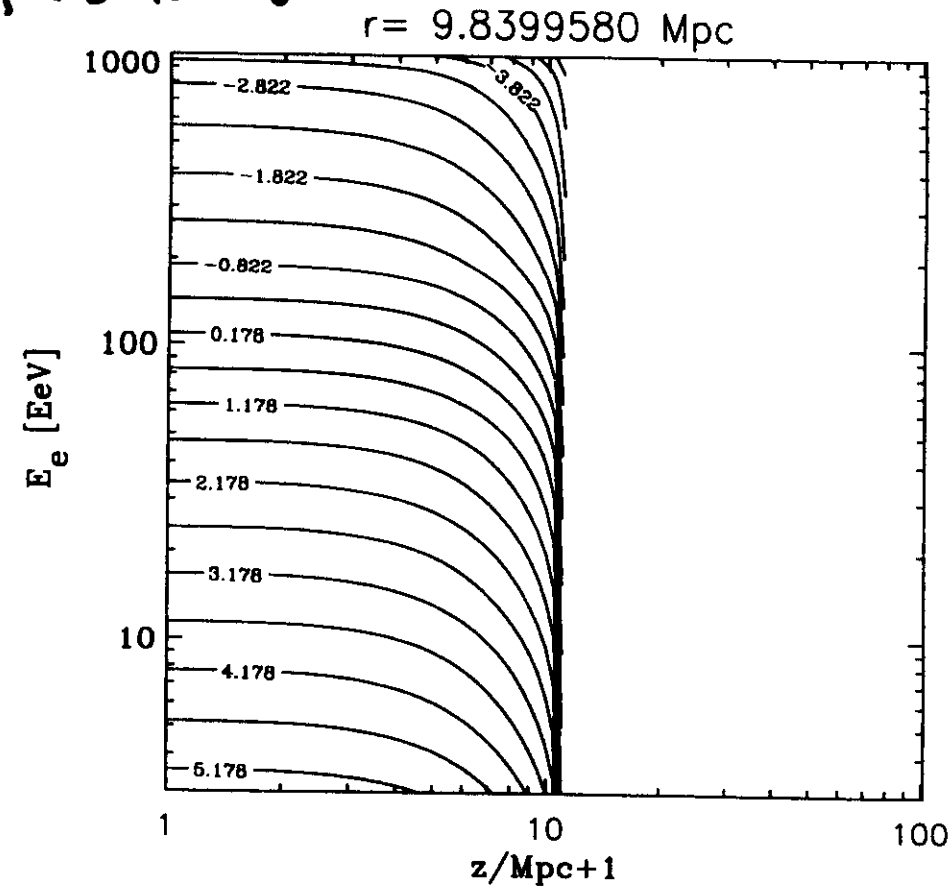

Sheet

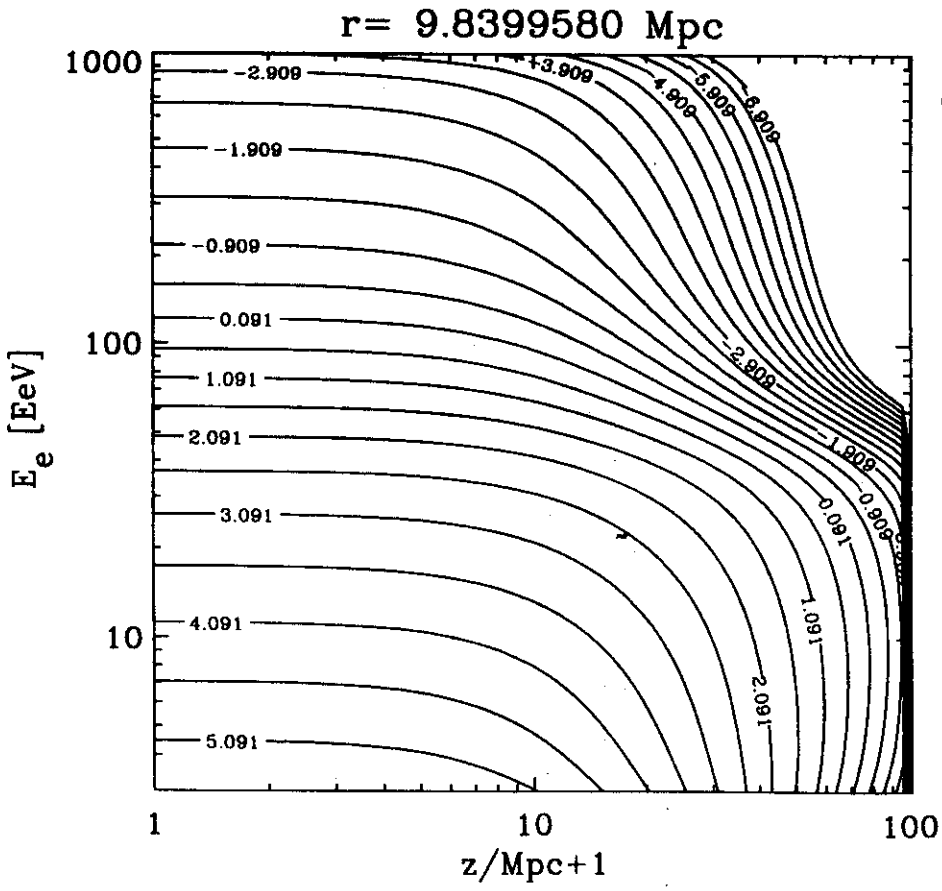

homogeneous

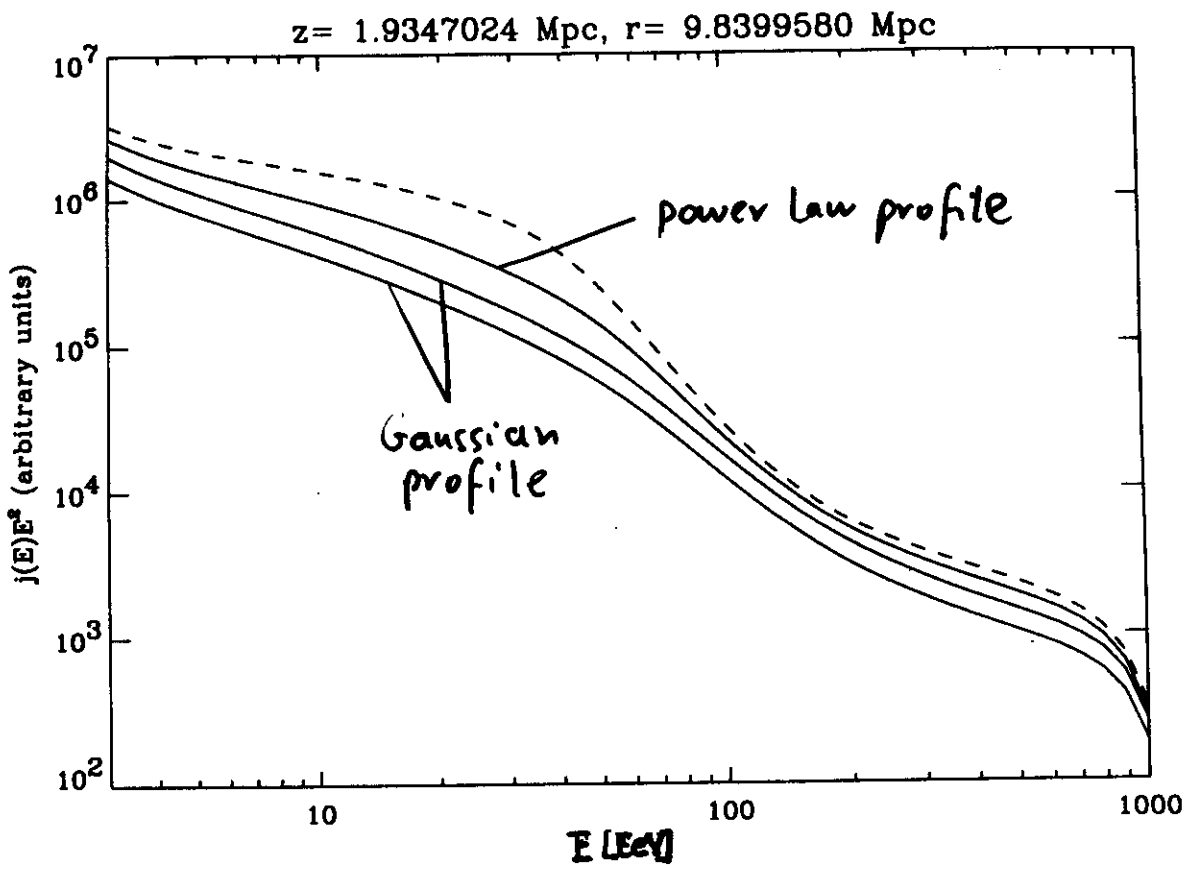

——— sheet — — — homogeneous

solution of diffusion - continuous energy loss equation

$B_{rms} = 5 \cdot 10^{-8}$ G , D ≈ 10 Mpc

confirms suppression

$D = 10$ Mpc $B_{rms} = 5 \cdot 10^{-8}$ G

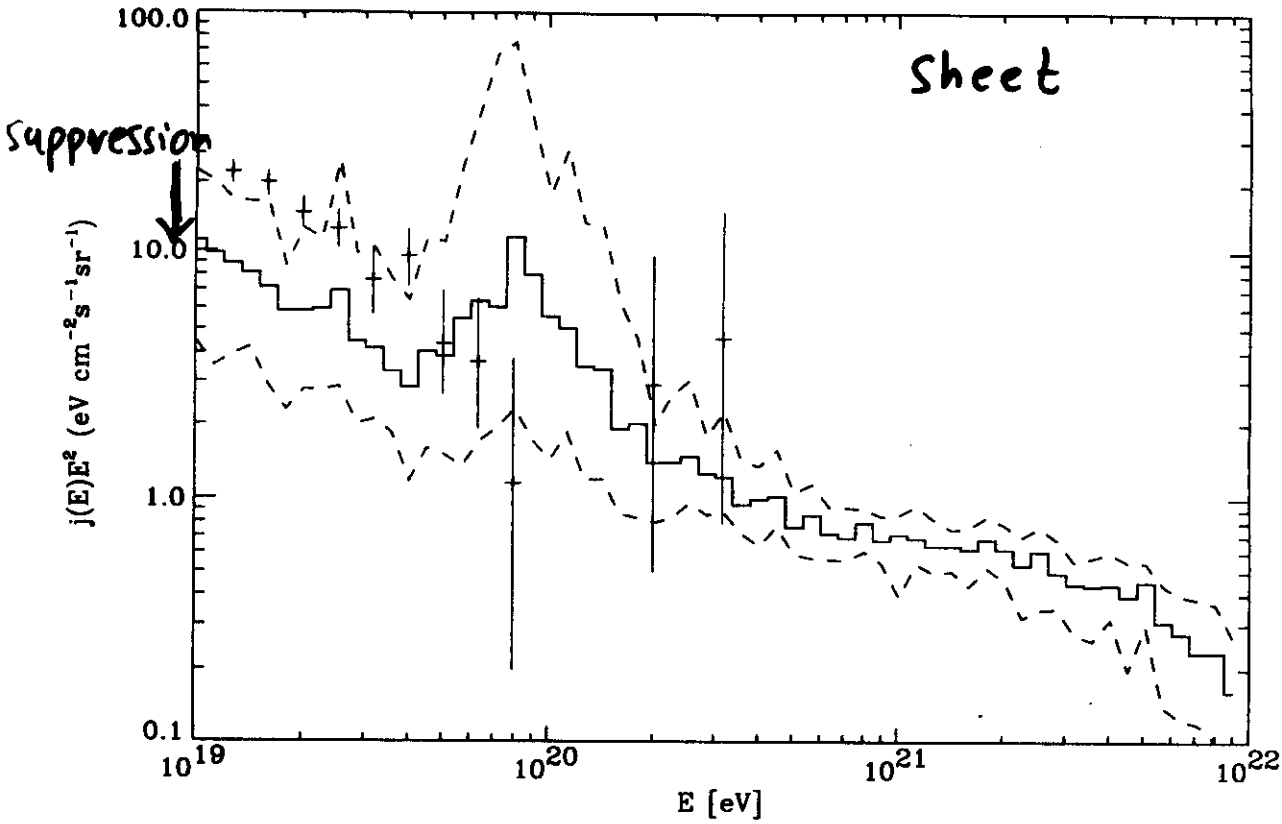

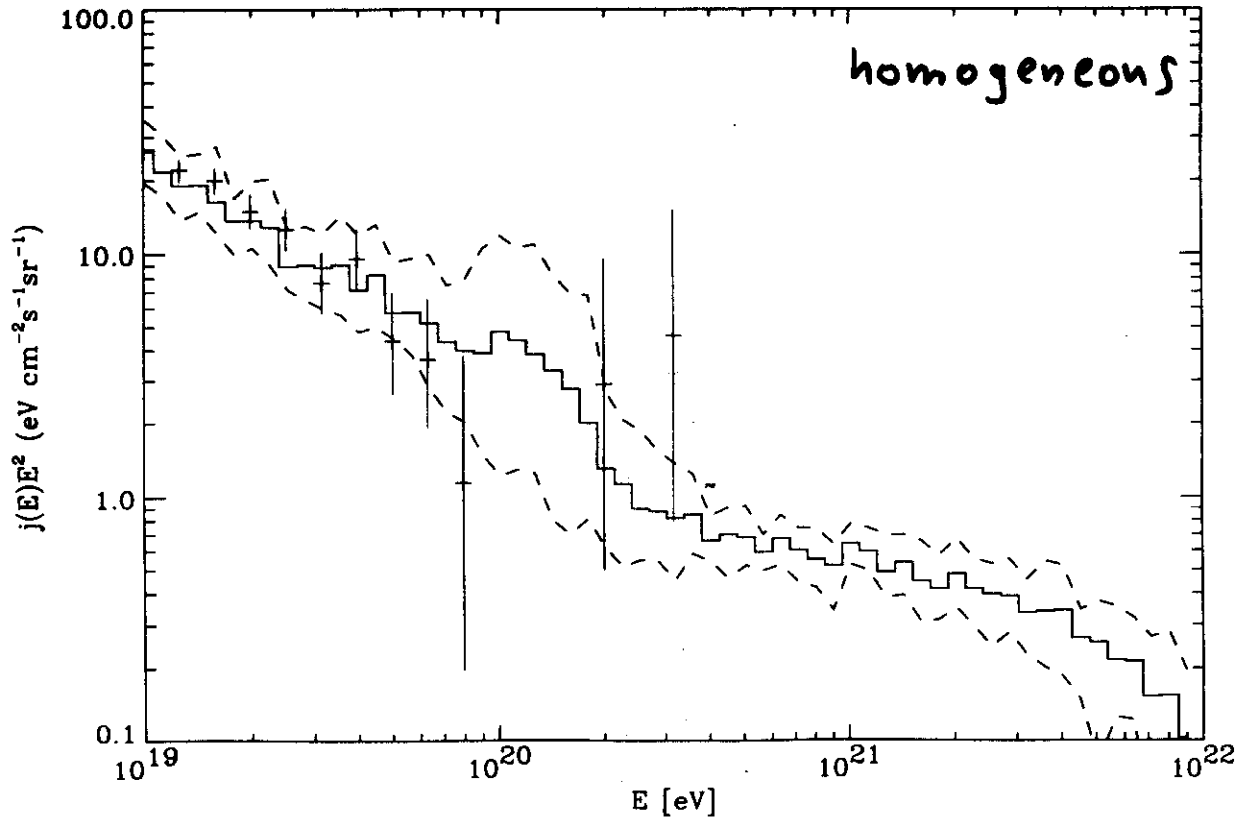

—— average — — — Standard deviation

$D = 10$ Mpc $\quad B_{rms} = 10^{-7}$ G

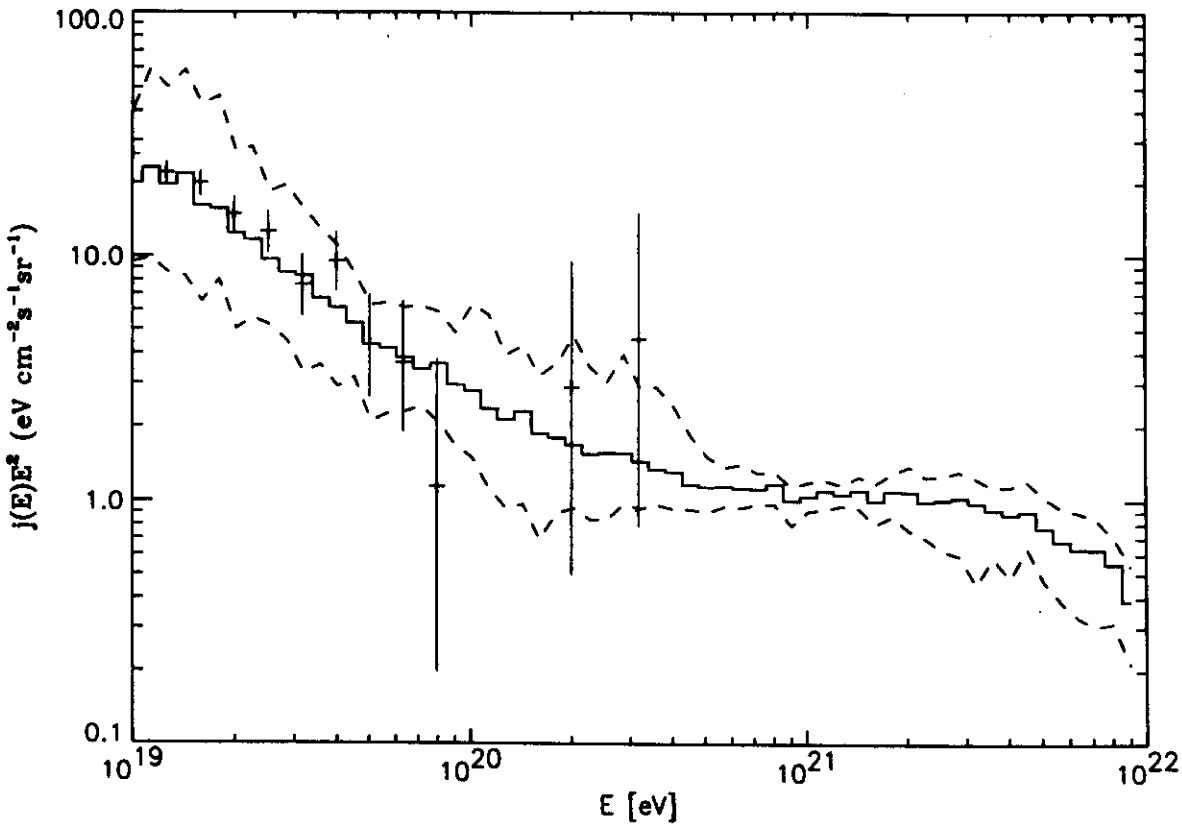

low energy depletion from sheet compensated by diffusively enhanced pion production

$\Longrightarrow$ best fit on average

$D = 10$ Mpc $B_{rms} = 3 \cdot 10^{-7}$ G

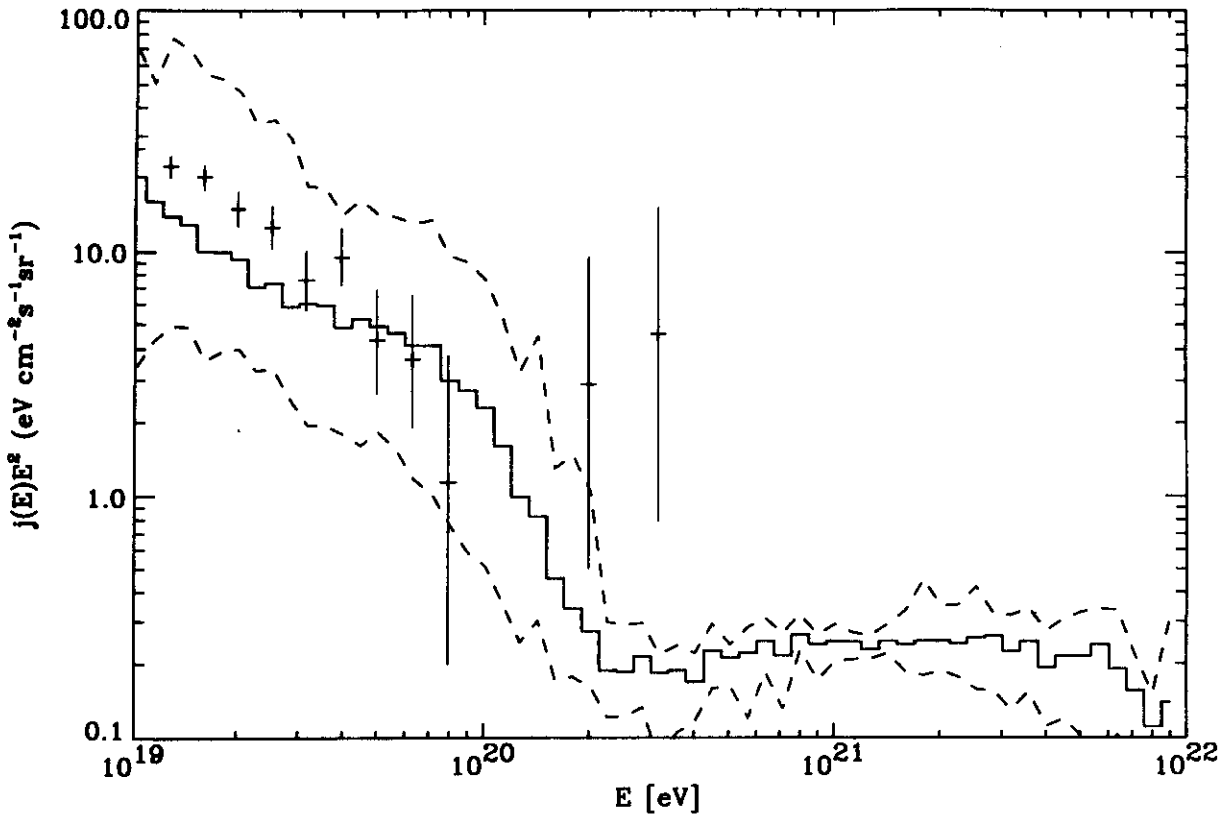

Low energy depletion from sheet overcompensated by diffusively enhanced pion production

$$B_{\rm rms,max} = 5 \times 10^{-8}\,{\rm G}$$

continuous source with $T_{\rm S} \gg \tau_{10} \sim 10^8\,{\rm yr}$, $j(E) \propto E^{-2.4}$ up to $10^{22}\,{\rm eV}$, $D = 10\,{\rm Mpc}$

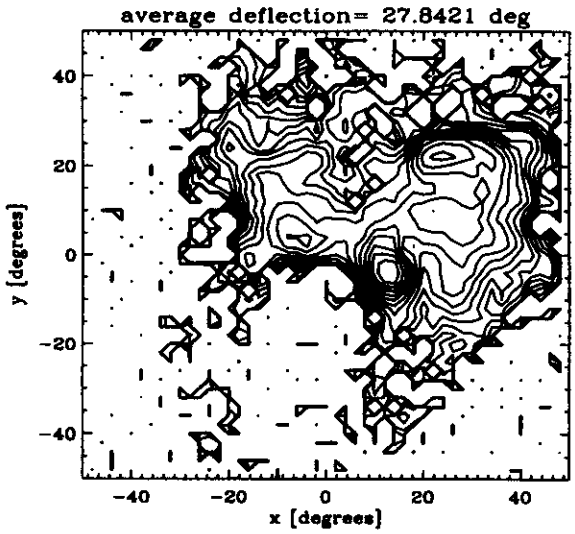

$E > 30\,{\rm EeV}$

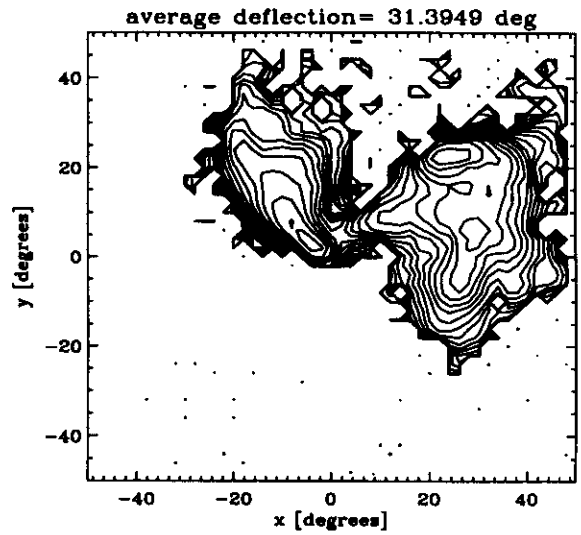

$E > 60\,{\rm EeV}$

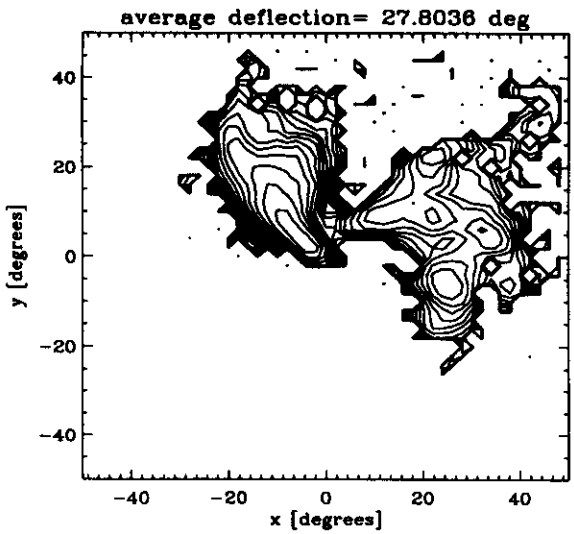

$E > 100\,{\rm EeV}$

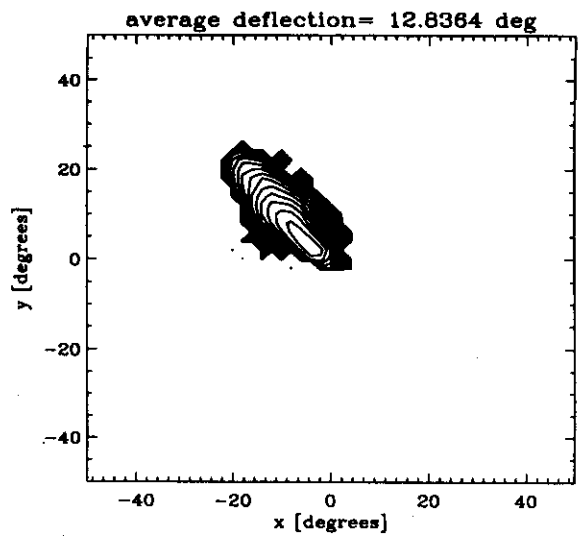

$E > 200\,{\rm EeV}$

$D\theta_E/l_c \simeq 1$ at $E \simeq 150\,{\rm EeV}$ $\Longrightarrow$ l_c can be estimated

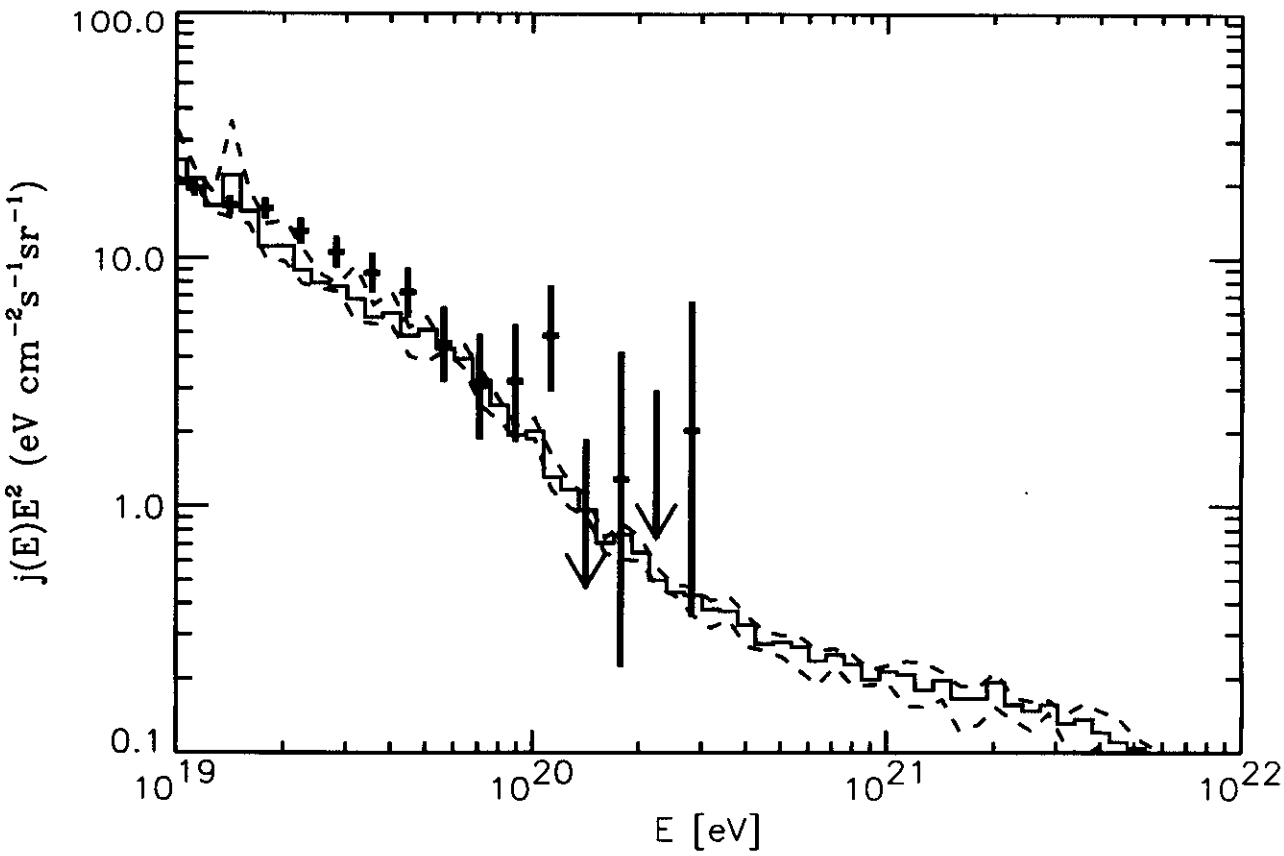
100.0
10.0
1.0
0.1
10^{19}
10^{20}
10^{21}
10^{22}
E [eV]
$j(E)E^2$ (eV cm^{-2}s^{-1}sr^{-1})

Supergalactic plane as a sheet with Gaussian profile, width=10 Mpc

Kolmogorov field with $B_{\rm rms,max} = 0.05 - 0.5\mu$G, $L_{\rm max} \simeq 10$ Mpc, $l_c \simeq 1$ Mpc

continuous source distribution follwing plane profile

with $T_S \gg \tau_{10} \sim 2 \times 10^8$ yr, $j(E) \propto E^{-2.4}$ up to 10^{22} eV

distance to center (Virgo) = 20 Mpc

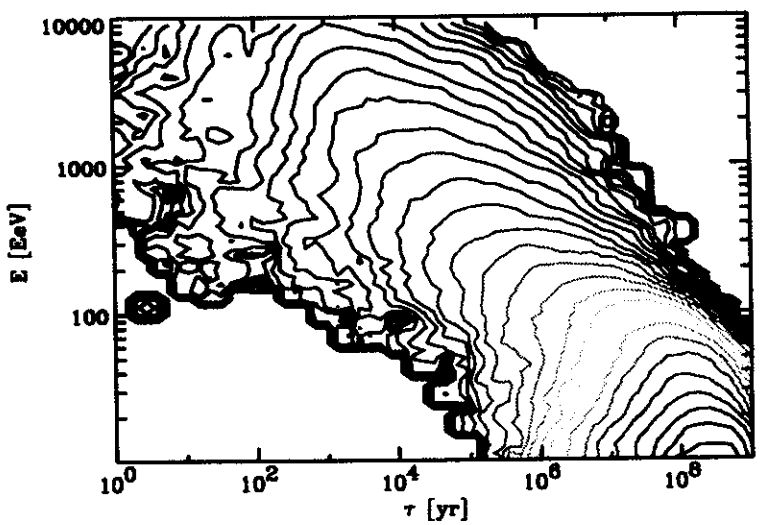

delay time-energy distribution

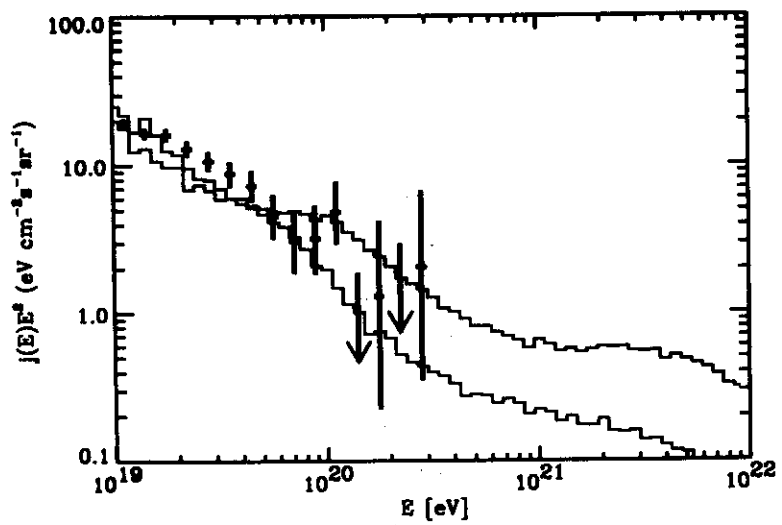

average spectrum: $B_{\rm rms,max} = 0.05/0.5\mu$G (blue/red)

cosmic variance negligible

Realization averaged angular distributions

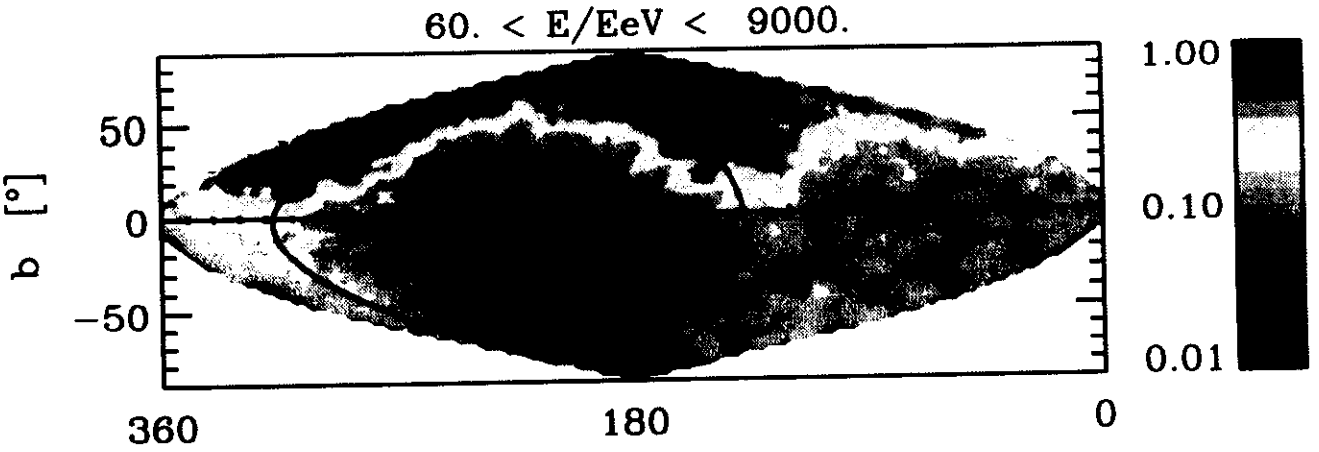

$B_{\rm rms,max} = 0.05\mu$ G, 20 Mpc source distribution radius

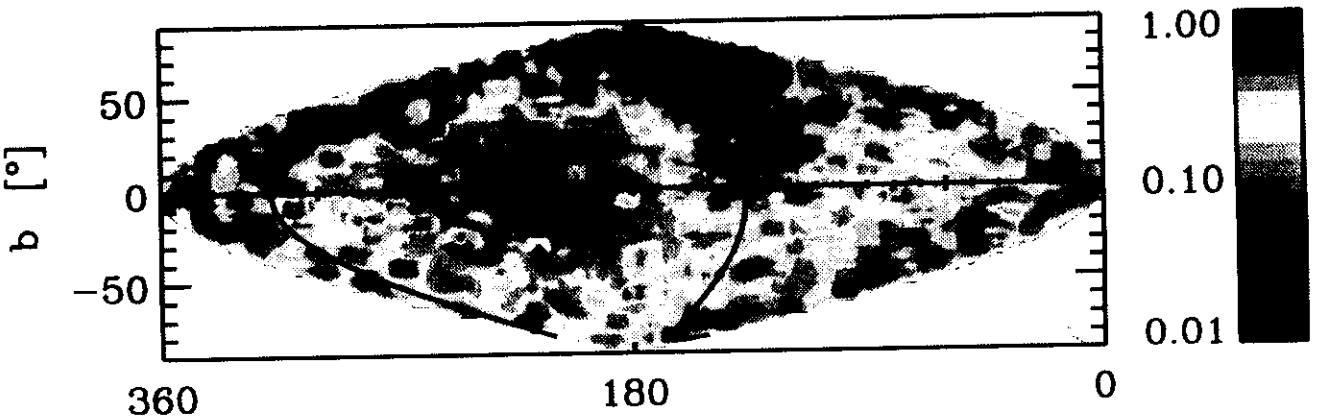

$B_{\rm rms,max} = 0.05\mu$ G, ∞ source distribution radius

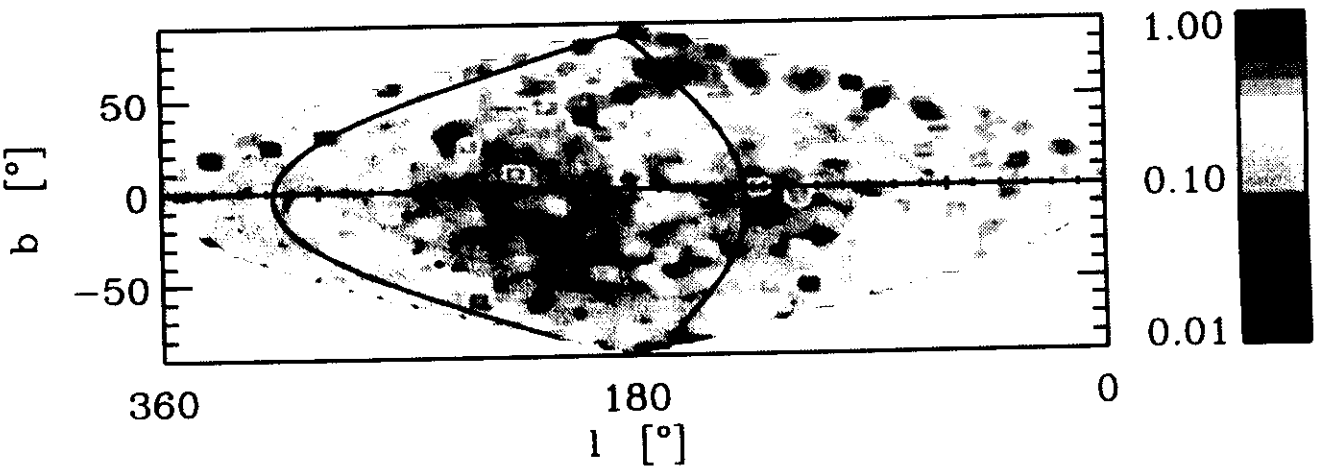

$B_{\rm rms,max} = 0.5\mu$ G, 20 Mpc source distribution radius

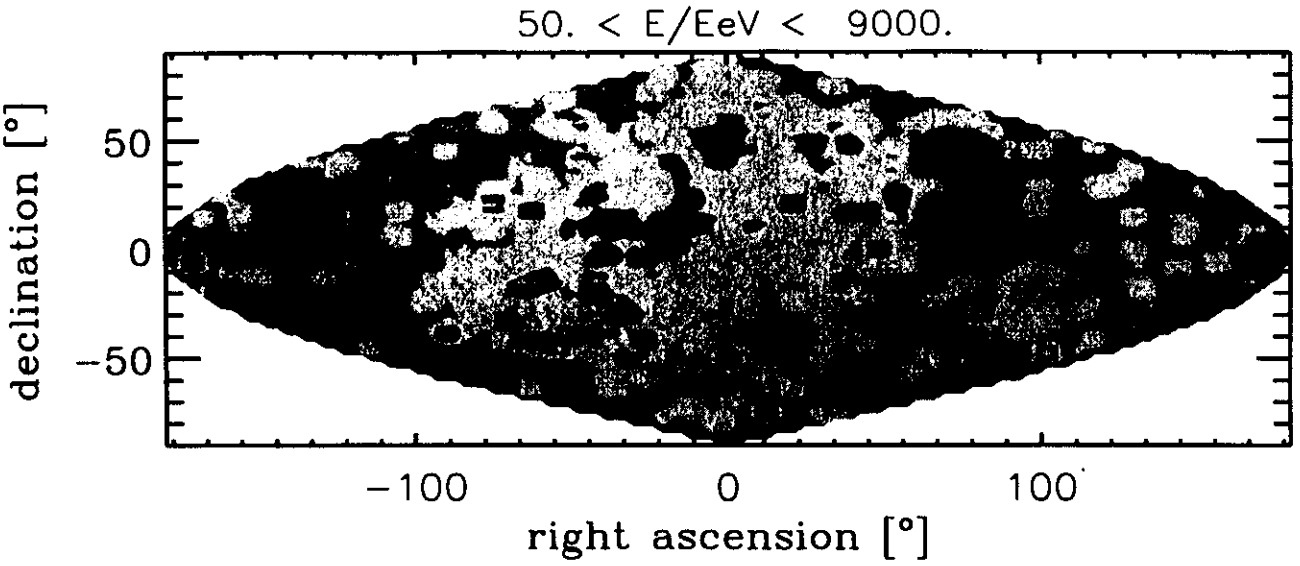
50. < E/EeV < 9000.
declination [°]
50
0
−50
−100
0
100
right ascension [°]

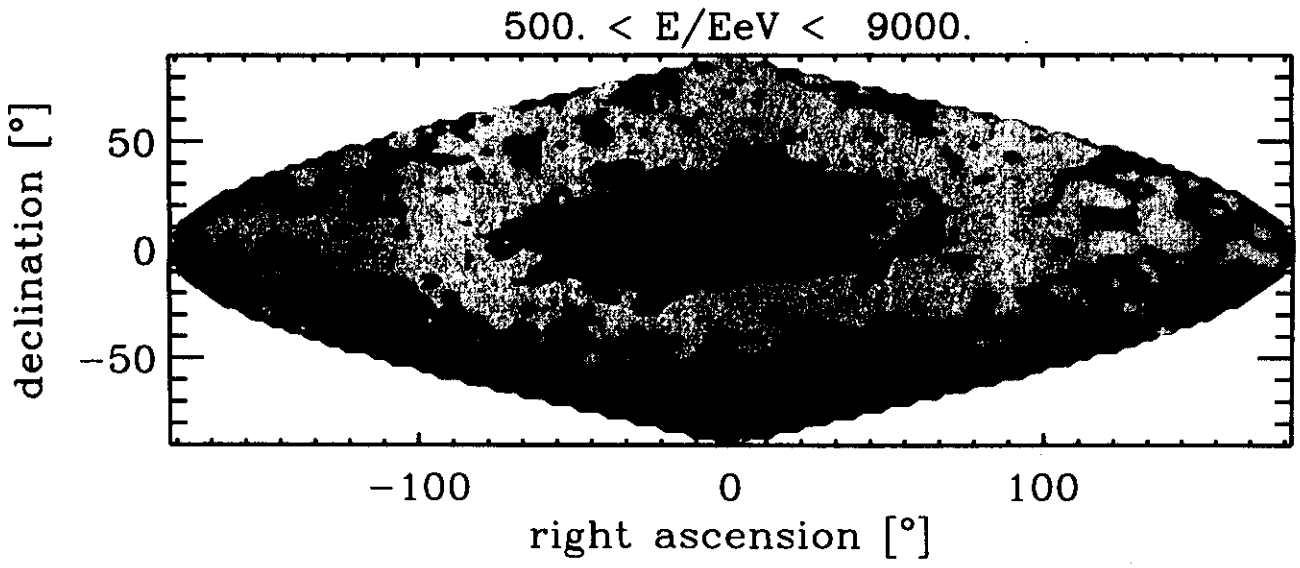
500. < E/EeV < 9000.
declination [°]
50
0
−50
−100
0
100
right ascension [°]

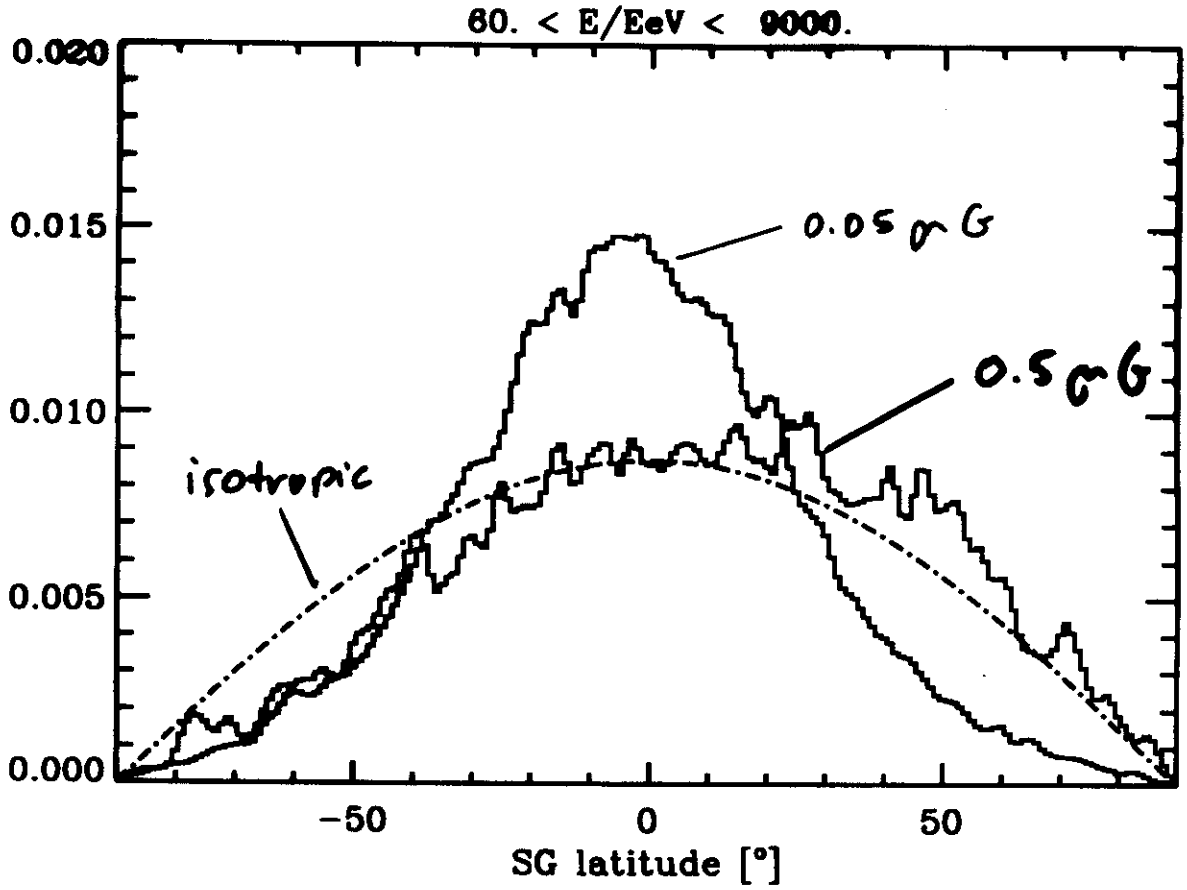

Realization averaged Supergalactic latitude distribution

for $B_{\rm rms,max} = 0.05/0.5\mu$G (blue/red)

Consequences:

Anisotropy decreases with increasing magnetic field strength due to diffusion and with increasing source distribution radius

Clustering increases with coherence and strength of magnetic field due to magnetic lensing and with increasing source distribution radius

Confidence levels strongly increase with exposure

Monte Carlo simulations of sources in a magnetized Supergalactic Plane

Kolmogorov spectrum with maximal field strength of 0.5 micro Gauss in plane center

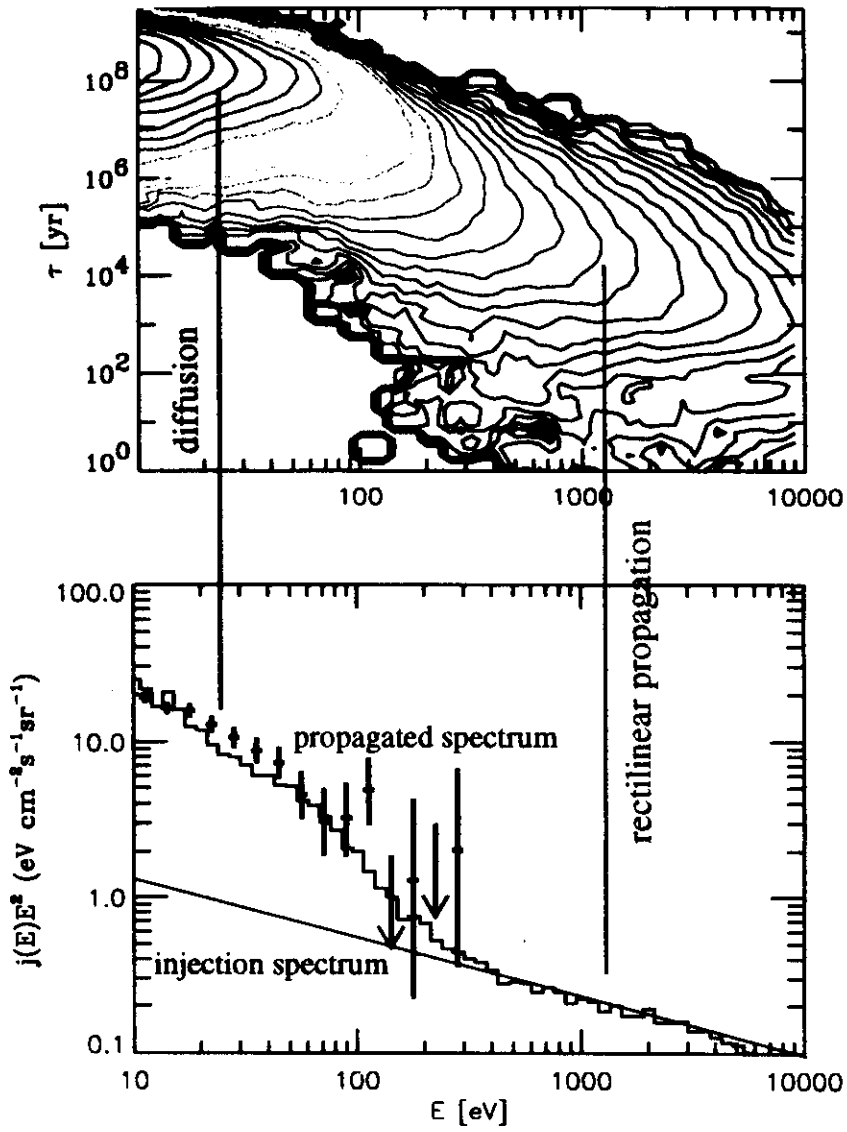

Angular distribution explains large scale isotropy (by diffusion) and small scale clustering (by magnetic lensing):